Copy 247
RM L56D17

RESEARCH MEMORANDUM

FORCE AND PRESSURE-DISTRIBUTION MEASUREMENTS AT A MACH NUMBER OF 3.12 OF SLENDER BODIES HAVING CIRCULAR, ELLIPTICAL, AND TRIANGULAR CROSS SECTIONS AND THE SAME LONGITUDINAL DISTRIBUTION OF CROSS-SECTIONAL AREA

By Roy H. Lange and Charles E. Wittliff

Langley Aeronautical Laboratory
Langley Field, Va.

NATIONAL ADVISORY COMMITTEE
FOR AERONAUTICS

WASHINGTON

July 13, 1956

[redacted]

NATIONAL ADVISORY COMMITTEE FOR AERONAUTICS

RESEARCH MEMORANDUM

FORCE AND PRESSURE-DISTRIBUTION MEASUREMENTS AT A MACH NUMBER OF 3.12 OF SLENDER BODIES HAVING CIRCULAR, ELLIPTICAL, AND TRIANGULAR CROSS SECTIONS AND THE SAME LONGITUDINAL DISTRIBUTION OF CROSS-SECTIONAL AREA

By Roy H. Lange and Charles E. Wittliff

SUMMARY

An investigation has been conducted at a Mach number of 3.12 and at a Reynolds number of 29×10^6 (based on body length) to determine the aerodynamic characteristics of bodies with elliptical and triangular cross sections and to compare these data with those of a related body having circular cross sections. The body having circular cross sections is the NACA RM-10 and the bodies with noncircular cross sections have the same longitudinal distribution of cross-sectional area as the NACA RM-10. Force tests to determine lift, drag, and pitching-moment characteristics as well as pressure-distribution measurements were made for an angle-of-attack range of ±8°.

INTRODUCTION

The theoretical work of Ferri, Ness, and Kaplita indicates that some reductions in drag at zero angle of attack can be obtained at supersonic speeds by the use of bodies having cross sections different from circular (ref. 1). At the present time, however, there are few systematic data available at supersonic speeds on the characteristics of related bodies with noncircular cross sections. (See refs. 2 to 4.) Therefore, the present investigation was undertaken on bodies with elliptical and triangular cross sections in order to compare the characteristics of these bodies with those of a body having circular cross sections. The body having the circular cross sections is the NACA RM-10 (without fins); the noncircular bodies have the same longitudinal distribution of cross-sectional area as that of the NACA RM-10.

[redacted]

[redacted]

The investigation was conducted in a blowdown jet located at the Langley gas dynamics laboratory at a Mach number of 3.12 and a Reynolds number of 29×10^6; hence, the data for the NACA RM-10 are extended to a higher Mach number than those obtained in references 5 to 7 while maintaining the same value of Reynolds number. Both force tests and pressure-distribution measurements were made on the bodies for a nominal angle-of-attack range of $\pm 8^\circ$. The lift, drag, pitching-moment, and pressure-distribution characteristics of the bodies are presented herein with a minimum of analysis in order to expedite release of this information.

SYMBOLS

Free-stream conditions:

ρ	mass density of air
V	airspeed
a	speed of sound in air
M	Mach number, V/a
q	dynamic pressure, $\frac{1}{2}\rho V^2$
p	static pressure
μ	viscosity of air
R	Reynolds number, $\frac{\rho VL}{\mu}$

Body geometry:

S	cross-sectional area
L	length of body
x	distance from nose of body measured along axis of symmetry
y	lateral coordinate, perpendicular to plane of symmetry
b	width of body
r	radius of NACA RM-10 body

f,g,h,w — cross-sectional dimensions of triangular body (see fig. 2)

d — semiminor axis of elliptical body

a — semimajor axis of elliptical body

K — geometric parameter

C — cross-sectional-area parameter of triangular body, $\sqrt{\frac{S_{max}}{\pi}}$

α — angle of attack of body center line, deg

θ — radial angle measured counterclockwise in plane perpendicular to axis of body when facing upstream ($\theta = 0^{\circ}$ on bottom of body in plane of angle of attack)

Force data:

C_L — lift coefficient, $\frac{\text{Lift}}{qS_{max}}$

C_N — normal-force coefficient, $\frac{\text{Normal force}}{qS_{max}}$

C_m — pitching-moment coefficient about nose of body, $\frac{\text{Pitching moment}}{qS_{max}L}$

C_D — forebody drag coefficient, $\frac{\text{Drag}}{qS_{max}}$

$\frac{C_L}{C_D}$ — lift-drag ratio

C_{L_α} — rate of change of lift coefficient with angle of attack, per degree

Pressure data:

p_l — local static pressure

P — pressure coefficient, $\frac{p_l - p}{q}$

c_n section normal-force coefficient, $\int_0^1 P_r d\left(\frac{2y}{b}\right)$

P_r resultant pressure coefficient, $P_{lower} - P_{upper}$

C_N normal-force coefficient, $\frac{2L}{\sqrt{\pi S_{max}}} \int_0^1 c_n K \, d\left(\frac{x}{L}\right)$ where K is as follows:

Body	K
NACA RM-10	r/r_{max}
Triangular	w/C
Elliptical (major axis vertical)	$d/\sqrt{a_{max} d_{max}}$
Elliptical (major axis horizontal)	$a/\sqrt{a_{max} d_{max}}$

Subscripts:

max maximum

N nominal or uncorrected

MODELS

The geometric characteristics of the three bodies tested are given in figures 1 and 2 and photographs of the bodies used in the pressure-distribution tests are given as figure 3. The body with the circular cross section is the NACA RM-10 with coordinates given by the equation in figure 1(a). The bodies with the elliptical and triangular cross sections have the same longitudinal distribution of cross-sectional area as that of the NACA RM-10. For the body with the elliptical cross section, the major axis is twice the minor axis.

Two sets of steel models were used - one set for the pressure-distribution tests and one set for the force tests. The body with triangular cross sections used in the force tests was made 15 percent larger than the dimensions given in figures 1 and 2 in order to accommodate the sting-supported internally mounted electrical strain-gage balance used in the force tests. For the pressure-distribution tests the bodies had 0.020-inch-diameter flush-surface static-pressure orifices arranged in sectionwise rows located 2, 4, 6, 8, 10, 12, and 14 inches from the body nose. The radial locations of the orifices, which are the same for all longitudinal stations, are indicated on the cross-sectional views of figure 2.

All models were sting supported. As shown in figure 3, the portion of the body rearward of the base (14.65-inch station) for each body used in the pressure-distribution tests was faired into a sting 1.5 inches long of constant area and with a cross-sectional shape the same as that of the body itself. For the body with the elliptical cross sections used in the presssure-distribution tests, a thin plate with wedge-shaped leading edges was required for strength at the model base. This plate eliminated the orifices at the 14-inch longitudinal station. No such plate was required for the body used in the force tests. The sting dimensions for the bodies are as follows:

Body	Characteristic dimension, in.
NACA RM-10 (pressure)	Diameter, 0.727
Triangular (pressure)	Total width, 0.748 Total height, 0.780
Elliptical (pressure)	Major axis, 1.005
NACA RM-10 (force)	Diameter, 0.576
Triangular (force)	Total width, 0.645 Total height, 0.685
Elliptical (force)	Major axis, 0.875

For the force models, four static-pressure orifices spaced 90° apart are provided on each sting at the 14.65-inch station for the measurement of the base pressure.

APPARATUS AND TESTS

The tests were conducted in a blowdown jet at the Langley gas dynamics laboratory having a two-dimensional nozzle with a rectangular test section approximately 9.5 inches high and 9 inches wide. The nozzle was designed by the method of characteristics with a correction made for boundary layer and operates at an average Mach number of 3.12. All the tests were made at a settling-chamber pressure of 150 pounds per square inch gage and at a stagnation dewpoint which eliminated any effect of condensation. The Reynolds number of the tests was approximately 23.7×10^6 per foot.

All tests were made through an angle-of-attack range from about -8° to 8° in increments of 2°. For the force tests, measurements were made at each angle of attack of the normal force, chord force, and pitching moment by means of a sting-supported electrical strain-gage balance internally mounted in the bodies. For the pressure-distribution tests, the surface static pressures were measured by means of a multiple-tube manometer and photographically recorded. The angles of attack were determined from schlieren photographs taken of the model for each test point. The angles of attack determined in this manner are accurate to within 0.10°.

For the pressure-distribution tests, the body with elliptical cross sections was tested through the angle-of-attack range both with the major axis vertical and with the major axis horizontal. For the force tests of the body with elliptical cross sections, the height of the three-component strain-gage balance was such that it could only be internally mounted in the body when alined with the major axis; hence, force tests could only be made of the body with the major axis vertical.

The base pressures measured were used to calculate the chord force acting at the base of the bodies, and the chord forces measured by the strain-gage balance were corrected to the condition of free-stream static pressure acting at the base of the bodies.

PRESENTATION OF RESULTS

The results of the investigation are given in figures 4 to 16 and in tables I to IV. The force measurements of each body are given as plots of C_L, C_m, C_D, and C_L/C_D against angle of attack in figures 4 to 6. A summary plot of C_D, C_L/C_D, and α against C_L is given in figure 7 for four body configurations for comparison purposes.

The data obtained from the pressure-distribution tests are presented in tables I, II, III, and IV for the NACA RM-10, the body with triangular cross sections, the body with elliptical cross sections and major axis vertical, and the body with elliptical cross sections and major axis horizontal, respectively. Nominal angles of attack α_N are used in the plots of the pressure-distribution data for convenience since the corrected angles of attack at each attitude are different for each body. These corrected angles of attack are given in tables I to IV.

The variation of pressure coefficient P with longitudinal position along the body x/L for the bodies with circular and elliptical cross sections is given in figure 8 for $\alpha_N = 0^\circ$ and $\theta = 0^\circ$ and 180°, and the effects of angle of attack are shown in figures 9 to 11. The pressure coefficients calculated by slender-body theory (see refs. 5 and 8) are superimposed on the experimental data of figure 8 at $\alpha_N = 0^\circ$; whereas, in figures 9 to 11, the calculated pressure coefficients for only the NACA RM-10 body are shown for comparison with the experimental data of the four bodies at angles of attack.

The variation of pressure coefficient with body width for four selected longitudinal stations and for angles of attack from 0° to 8° are given in figure 12. These plots, together with those for longitudinal stations not presented, were integrated to obtain the local normal-force coefficients for the bodies. The variation of pressure coefficient with radial angle for four selected longitudinal stations and for angles of attack from 0° to 6° are presented in figure 13 for the NACA RM-10 body and are compared with the predictions of slender-body theory. Similar data for the body with elliptical cross sections at 0° angle of attack are given in figure 14.

The longitudinal distribution of section loading parameter c_nK is presented in figure 15 for the four body configurations at angles of attack of 2°, 4°, 6°, and 8°. Integration of the curves of figure 15 yields the total normal-force coefficient as obtained from the pressure-distribution tests; however, sufficient data were available only for the NACA RM-10 and for the body with triangular cross sections, and these values of C_N are compared in figure 16 with those obtained on the bodies from force tests.

DISCUSSION OF RESULTS

Although no detailed discussion of the results of the investigation will be attempted in this paper, the results of most interest will be briefly pointed out in the paragraphs that follow.

The results of the force tests of the bodies are summarized in the following table:

Body	C_{L_α} ($\alpha = 0^\circ$)	C_D ($C_L = 0$)	C_L/C_D ($C_L = 0.2$)	C_L/C_D ($C_L = 0.4$)
NACA RM-10	0.0323	0.086	1.88	2.83
Triangular (upright)	.0460	.118	1.38	2.16
Triangular (inverted)	.0460	.118	1.59	2.63
Elliptical (vertical)	.0217	.094	1.43	----

It is interesting to note that the body with circular cross sections (NACA RM-10) has the lowest drag. Slender-body theory (ref. 8) predicts lower wave drag for the body with elliptical cross sections than for the equivalent body of revolution, although the difference is small for the bodies considered here. For the test conditions reported herein, it is estimated that the skin-friction drag is about 70 percent of the total drag and if the skin-friction drag is subtracted from the total drag, then the remainder of the drag can be considered as indicative of the wave-drag level for each body. These remainders agree within 4 percent for the elliptical- and circular-cross-section bodies; therefore, it is felt that the tests agree with the slender-body theory to the extent that the differences in wave drag between the elliptical- and circular-cross-section bodies are small.

Above a lift coefficient of 0.15, the inverted body with triangular cross sections had the highest values of lift-drag ratio of the noncircular bodies tested, and, at $C_L = 0.4$, this value was only 7 percent lower than that of the NACA RM-10 body. (See fig. 7.) These larger values of lift-drag ratio of the inverted body with triangular cross sections are a result of the relatively low drag rise with increase in lift, even when comparison is made with the NACA RM-10 data. It should be noted that had force tests been made on the elliptical body (horizontal) it probably would have attained the highest C_L/C_D values because of an improved lift-curve slope. This improved lift-curve slope is indicated for the elliptical body (horizontal) in the section-loading curves of figure 15. The use of cross-flow theory (ref. 9) improves the correlation between the calculated and experimental aerodynamic characteristics of the NACA RM-10 over that obtained with slender-body theory, as expected; however, the agreement is poor throughout. (See fig. 4.) The minimum drag coefficients of the NACA RM-10 and of the body with elliptical cross sections are overestimated by 15 percent and 12 percent, respectively, by the slender-body (potential) theory and this is due mainly to the assumption of a turbulent boundary layer over the entire length of the body in calculating the skin-friction drag.

There are significant differences in the sectionwise distribution of static pressures among the different cross-section shapes investigated near the nose of the bodies (see fig. 12); however, at a given attitude, these differences become less pronounced with increase in distance along the body from the nose. In general, the body with elliptical cross sections and with the major axis horizontal has a pressure distribution which is rectangular in shape, the NACA RM-10 has an elliptical distribution, the body with triangular cross sections has a triangular distribution at the outer edges, and the body with elliptical cross sections and major axis vertical has a triangular distribution. The effect of increasing angle of attack is to amplify these differences in pressure distributions for longitudinal stations ahead of the maximum thickness of the body (fig. 12).

The agreement between the pressures predicted by slender-body (potential) theory and those obtained from the experiments is good near the nose at zero angle of attack for the NACA RM-10 and for the body with elliptical cross sections; however, the agreement is poor for stations near and rearward of the maximum thickness. (See figs. 8, 13(a), and 14.)

A comparison of the normal-force coefficients obtained from force measurements with those obtained from pressure-distribution measurements shows good agreement for the NACA RM-10 but only fair agreement for the body with triangular cross sections. This fair agreement of the data for the body with triangular cross sections results from the uncertainty in the fairing of the sectionwise pressure distributions especially at the outer edges of the body.

Langley Aeronautical Laboratory,
National Advisory Committee for Aeronautics,
Langley Field, Va., April 3, 1956.

REFERENCES

1. Ferri, Antonio, Ness, Nathan, and Kaplita, Thaddeus T.: Supersonic Flow Over Conical Bodies Without Axial Symmetry. Jour. Aero. Sci., vol. 20, no. 8, Aug. 1953, pp. 563-571.

2. Carlson, Harry W., and Gapcynski, John P.: An Experimental Investigation at a Mach Number of 2.01 of the Effects of Body Cross-Section Shape on the Aerodynamic Characteristics of Bodies and Wing-Body Combinations. NACA RM L55E23, 1955.

3. Ridyard, Herbert W.: The Aerodynamic Characteristics of Two Series of Lifting Bodies at Mach Number 6.86. NACA RM L54C15, 1954.

4. Stoney, William E., Jr., and Putland, Leonard W.: Some Effects of Body Cross-Sectional Shape, Including a Sunken-Canopy Design, on Drag as Shown by Rocket-Powered Model Tests at Mach Numbers From 0.8 to 1.5. NACA RM L52D07, 1952.

5. Luidens, Roger W., and Simon, Paul C.: Aerodynamic Characteristics of NACA RM-10 Missile in 8- by 6-Foot Supersonic Wind Tunnel at Mach Numbers From 1.49 to 1.98. I - Presentation and Analysis of Pressure Measurements (Stabilizing Fins Removed). NACA RM E50D10, 1950.

6. Esenwein, Fred T., Obery, Leonard J., and Schueller, Carl F.: Aerodynamic Characteristics of NACA RM-10 Missile in 8- by 6-Foot Supersonic Wind Tunnel at Mach Numbers From 1.49 to 1.98. II - Presentation and Analysis of Force Measurements. NACA RM E50D28, 1950.

7. Luidens, Roger W., and Simon, Paul C.: Aerodynamic Characteristics of NACA RM-10 Missile in 8- by 6-Foot Supersonic Wind Tunnel at Mach Numbers From 1.49 to 1.98. III - Analysis of Force Distribution at Angle of Attack (Stabilizing Fins Removed). NACA RM E50I19, 1950.

8. Kahane, A., and Solarski, A.: Supersonic Flow About Slender Bodies of Elliptic Cross Section. Jour. Aero. Sci., vol. 20, no. 8, Aug. 1953, pp. 513-524.

9. Allen, H. Julian: Estimation of the Forces and Moments Acting on Inclined Bodies of Revolution of High Fineness Ratio. NACA RM A9I26, 1949.

TABLE I.— PRESSURE COEFFICIENT DATA FOR RM-10 BODY

(a) Positive angles of attack

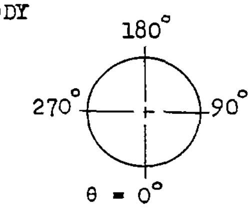

α, deg	Station, x/L	Radial angle, θ, deg						
		90	120	150	180	210	240	270
0.1	0.137	0.0364	0.0405	0.0373	0.0343	0.0360	0.0364	0.0317
	.273	—	.0161	.0182	.0191	.0152	.0178	.0186
	.410	.0009	.0028	.0047	.0054	.0054	.0041	—
	.546	-.0062	-.0088	-.0088	-.0109	-.0107	-.0152	-.0084
	.683	-.0204	-.0141	-.0156	-.0152	—	-.0167	-.0195
	.819	-.0229	-.0246	-.0246	-.0191	-.0195	-.0248	-.0219
	.956	-.0223	-.0223	-.0221	-.0219	-.0201	-.0227	-.0206
2.3	.137	.0347	.0313	.0227	.0197	.0214	.0270	.0300
	.273	—	.0096	.0107	.0107	.0077	.0111	.0163
	.410	-.0004	-.0051	-.0064	-.0051	-.0051	-.0039	—
	.546	-.0124	-.0137	-.0081	-.0107	-.0090	-.0206	-.0150
	.683	-.0004	-.0184	-.0193	-.0176	—	-.0197	-.0184
	.819	-.0304	-.0257	-.0227	-.0210	-.0231	-.0270	-.0287
	.956	-.0240	-.0193	-.0171	-.0163	-.0167	-.0201	-.0219
4.2	.137	.0291	.0214	.0137	.0120	.0124	.0176	.0236
	.273	—	-.0017	-.0009	-.0004	-.0039	-.0013	-.0094
	.410	-.0124	-.0150	-.0077	-.0056	-.0081	-.0146	—
	.546	-.0176	-.0184	-.0111	-.0150	-.0099	-.0274	-.0219
	.683	-.0081	-.0270	-.0227	-.0206	—	-.0300	-.0317
	.819	-.0403	-.0291	-.0240	-.0214	-.0240	-.0309	-.0403
	.956	-.0399	-.0279	-.0219	-.0167	-.0214	-.0240	-.0279
6.2	.137	.0144	.0011	-.0024	-.0024	-.0049	-.0028	-.0088
	.273	—	-.0152	-.0066	-.0045	-.0101	-.0139	-.0075
	.410	-.0246	-.0234	-.0174	-.0139	-.0178	-.0281	—
	.546	-.0390	-.0351	-.0184	-.0231	-.0189	-.0412	-.0454
	.683	-.0360	-.0369	-.0309	-.0270	—	-.0416	-.0544
	.819	-.0591	-.0381	-.0356	-.0261	-.0360	-.0381	-.0634
	.956	-.0351	-.0339	-.0381	-.0231	-.0343	-.0334	-.0347
8.3	.137	.0047	-.0116	-.0060	-.0036	-.0090	-.0148	-.0013
	.273	—	-.0326	-.0156	-.0124	-.0180	-.0304	-.0176
	.410	-.0420	-.0437	-.0270	-.0219	-.0279	-.0463	—
	.546	-.0617	-.0429	-.0283	-.0227	-.0294	-.0484	-.0642
	.683	-.0561	-.0416	-.0420	-.0266	—	-.0435	-.0767
	.819	-.0531	-.0467	-.0531	-.0334	-.0510	-.0474	-.0572
	.956	-.0405	-.0456	-.0546	-.0405	-.0465	-.0418	-.0381

TABLE I.– PRESSURE COEFFICIENT DATA FOR RM-10 BODY

(b) Negative angles of attack

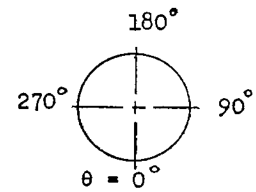

α, deg	Station, x/L	Radial angle, θ, deg						
		270	300	330	0	30	60	90
-0.2	0.137	.0345	.0401	.0371	.0345	.0362	.0375	.0319
	.273	—	.0161	.0182	.0191	.0152	.0178	.0186
	.410	.0006	.0028	.0045	.0054	.0054	.0032	—
	.546	-.0064	-.0090	-.0094	-.0111	-.0004	-.0163	-.0090
	.683	-.0009	-.0146	-.0159	-.0154	—	-.0167	-.0197
	.819	-.0236	-.0249	-.0249	-.0240	-.0210	-.0236	-.0223
	.956	-.0223	-.0223	-.0223	-.0219	-.0206	-.0227	-.0209
-2.1	.137	.0334	.0467	.0488	.0501	.0493	.0433	.0296
	.273	—	.0201	.0309	.0339	.0274	.0219	.0150
	.410	.0030	.0026	.0094	.0129	.0099	.0030	—
	.546	-.0103	-.0056	-.0017	-.0009	-.0021	-.0150	-.0137
	.683	-.0249	-.0210	-.0201	-.0180	—	-.0236	-.0249
	.819	-.0261	-.0270	-.0253	-.0227	-.0249	-.0274	-.0244
	.956	-.0253	-.0300	-.0300	-.0291	-.0279	-.0291	-.0291
-4.1	.137	.0249	.0471	.0634	.0686	.0626	.0474	.0208
	.273	—	.0219	.0437	.0508	.0396	.0240	.0090
	.410	-.0120	.0039	.0208	.0283	.0204	.0039	—
	.546	-.0242	-.0120	.0036	.0088	.0019	-.0216	-.0281
	.683	-.0319	-.0255	-.0156	-.0081	—	-.0294	-.0311
	.819	-.0437	-.0384	-.0255	-.0195	-.0274	-.0399	-.0403
	.956	-.0309	-.0437	-.0360	-.0296	-.0360	-.0414	-.0231
-6.6	.137	.0169	.0506	.0803	.0869	.0780	.0530	.0129
	.273	—	.0219	.0579	.0698	.0536	.0201	-.0039
	.410	-.0257	.0009	.0300	.0424	.0281	—	—
	.546	-.0328	-.0161	.0096	.0186	.0075	-.0255	-.0377
	.683	-.0506	-.0291	-.0088	.0017	—	-.0341	-.0486
	.819	-.0593	-.0495	-.0276	-.0191	-.0300	-.0527	-.0538
	.956	-.0321	-.0589	-.0360	-.0257	-.0399	-.0548	-.0283

TABLE II. - PRESSURE COEFFICIENT DATA FOR TRIANGULAR BODY

(a) Positive angles of attack

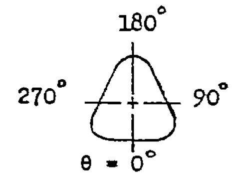

α, deg	Station x/L	Radial angle, θ, deg 0	16.5	30.7	48.4	66.3	86.2	111.4	144.2	162.4	180
0.1	0.137	.0283	.0302	.0296	.0343	.0279	.0328	.0317	.0347	—	.0339
	.273	.0141	—	.0148	.0066	.0191	.0161	.0159	.0178	.0223	.0231
	.546	—	-.0161	—	—	-.0054	-.0077	-.0090	-.0137	-.0137	-.0090
	.683	-.0208	-.0204	-.0114	-.0103	.0118	.0206	-.0135	-.0133	-.0137	-.0150
	.819	-.0240	-.0212	-.0212	—	-.0216	-.0221	-.0234	-.0219	-.0223	—
	.956	-.0229	-.0227	-.0225	-.0165	-.0208	-.0216	-.0219	-.0227	-.0238	-.0212
2.4	.137	.0433	.0456	.0446	.0330	.0169	.0219	.0216	.0208	.0249	.0159
	.273	.0249	—	.0240	.0047	.0079	.0060	.0056	.0081	.0118	.0090
	.546	—	-.0081	—	—	-.0122	-.0135	-.0135	-.0144	-.0139	-.0129
	.683	-.0212	-.0201	-.0081	-.0096	.0122	.0212	-.0126	-.0159	-.0176	-.0174
	.819	-.0272	-.0255	-.0236	—	-.0257	-.0255	-.0244	-.0210	-.0212	—
	.956	-.0313	-.0309	-.0291	-.0279	-.0257	-.0246	-.0240	-.0227	-.0197	-.0171
4.4	.137	.0673	.0694	.0686	.0339	.0109	.0197	.0184	.0195	—	.0133
	.273	.0456	—	.0435	.0079	.0043	.0047	.0036	.0041	.0056	.0026
	.546	—	.0004	—	—	-.0165	-.0126	-.0129	-.0159	-.0184	-.0126
	.683	-.0131	-.0126	-.0006	-.0159	.0135	.0225	-.0201	-.0195	-.0184	-.0195
	.819	-.0302	-.0291	-.0306	—	-.0317	-.0287	-.0264	-.0236	-.0208	—
	.956	-.0334	-.0345	-.0330	-.0381	-.0315	-.0306	-.0279	-.0227	-.0180	-.0146
6.5	.137	.0904	.0921	.0895	.0210	-.0047	.0060	.0064	.0066	—	.0004
	.273	.0673	—	.0619	.0019	-.0167	-.0073	-.0043	-.0011	-.0009	-.0017
	.546	—	.0124	—	—	-.0324	-.0253	-.0214	-.0208	-.0253	-.0191
	.683	-.0077	-.0088	.0103	-.0403	.0126	.0216	-.0289	-.0253	-.0229	-.0236
	.819	-.0236	-.0244	-.0283	—	-.0463	-.0471	-.0398	-.0287	-.0231	—
	.956	-.0439	-.0458	-.0469	-.0585	-.0461	-.0497	-.0497	-.0296	-.0189	-.0124
8.3	.137	.1185	.1198	.1148	.0129	-.0195	-.0002	.0019	.0034	—	-.0002
	.273	.0902	—	.08333	.0026	-.0309	-.0148	-.0109	-.0090	-.0071	-.0079
	.546	—	.0304	—	—	-.0548	-.0497	-.0345	-.0291	-.0236	-.0186
	.683	.0077	.0056	.0274	-.0578	-.0407	-.0369	-.0369	-.0246	-.0216	-.0216
	.819	-.0131	-.0144	-.0204	—	-.0602	-.0701	-.0688	-.0276	-.0229	—
	.956	-.0384	-.0409	-.0452	-.0701	-.0581	-.0589	-.0808	-.0450	-.0195	-.0133

TABLE II.– PRESSURE COEFICIENT DATA FOR TRIANGULAR BODY

(b) Negative angles of attack

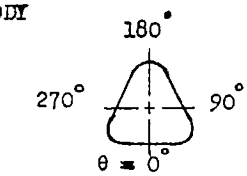

α, deg	Station x/L	Radial angle, θ, deg: 0	16.5	30.7	48.4	66.3	86.2	111.4	144.2	162.4	180
0.1	0.137	.0283	.0302	.0296	.0343	.0279	.0328	.0317	.0347	—	.0339
	.273	.0141	—	.0148	.0066	.0191	.0161	.0159	.0178	.0223	.0231
	.546	—	–.0161	—	—	–.0054	–.0077	–.0090	–.0137	–.0137	–.0090
	.683	–.0208	–.0204	–.0114	–.0103	.0118	.0206	–.0135	–.0133	–.0137	–.0150
	.819	–.0240	–.0212	–.0212	—	–.0216	–.0221	–.0234	–.0219	–.0223	—
	.956	–.0229	–.0227	–.0225	–.0165	–.0208	–.0216	–.0219	–.0227	–.0238	–.0212
–1.9	.137	.0159	.0171	.0163	.0261	.0317	.0390	.0398	.0441	—	.0561
	.273	.0049	—	.0049	–.0021	.0171	.0184	.0214	.0257	.0300	.0390
	.546	—	–.0189	—	—	–.0103	–.0069	–.0056	–.0090	–.0069	0
	.683	–.0171	–.0169	–.0167	–.0174	–.0227	–.0167	–.0176	–.0165	–.0163	–.0165
	.819	–.0229	–.0231	–.0225	—	–.0302	–.0242	–.0238	–.0234	–.0221	—
	.956	–.0199	–.0199	–.0216	–.0249	–.0326	–.0330	–.0328	–.0315	–.0285	–.0255
–3.9	.137	.0066	.0075	.0060	.0118	.0317	.0422	.0456	.0521	—	.0754
	.273	–.0028	—	–.0049	–.0154	.0161	.0238	.0287	.0339	.0405	.0555
	.546	—	–.0174	—	—	–.0199	–.0105	–.0064	–.0071	–.0024	.0109
	.683	–.0225	–.0225	–.0174	–.0296	–.0319	–.0186	–.0152	–.0133	–.0131	–.0114
	.819	–.0270	–.0283	–.0317	—	–.0463	–.0339	–.0296	–.0236	–.0193	—
	.956	–.0266	–.0266	–.0291	–.0261	–.0381	–.0373	–.0369	–.0356	–.0317	–.0261
–5.8	.137	–.0032	–.0028	–.0051	–.0090	.0321	.0499	.0568	.0641	—	.0975
	.273	–.0103	—	–.0163	–.0366	.0071	.0251	.0349	.0435	.0553	.0765
	.546	—	–.0244	—	—	–.0249	–.0058	–.0009	–.0013	.0017	.0204
	.683	–.0296	–.0281	–.0317	–.0394	–.0458	–.0208	–.0111	–.0062	–.0056	.0009
	.819	–.0351	–.0369	–.0437	—	–.0583	–.0358	–.0294	–.0244	–.0210	—
	.956	–.0446	–.0450	–.0433	–.0315	–.0392	–.0416	–.0388	–.0347	–.0306	–.0227

TABLE III.- PRESSURE COEFFICIENT DATA FOR ELLIPTICAL BODY.
MAJOR AXIS VERTICAL

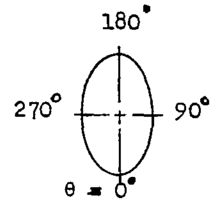

α, deg	Station x/L	Radial angle, θ, deg: 0	10	20	45	90	180	190	200	225	270
0.1	0.137	.0439	.0403	.0371	.0311	.0268	.0411	.0364	.0373	.0296	.0276
	.546	-.0114	—	-.0066	-.0084	-.0109	-.0111	-.0090	-.0135	-.0107	-.0079
	.819	-.0178	-.0219	-.0227	-.0199	-.0221	-.0234	-.0234	-.0246	-.0255	-.0216
2.6	.137	.0613	.0525	.0463	.0351	.0279	.0259	.0257	.0279	.0253	.0268
	.546	-.0024	—	-.0006	-.0088	-.0139	-.0096	-.0077	-.0120	-.0139	-.0126
	.819	-.0171	-.0210	-.0219	-.0240	-.0270	-.0210	-.0212	-.0238	-.0272	-.0266
4.3	.137	.0840	.0688	.0576	.0371	.0270	.0171	.0180	.0197	.0210	.0242
	.546	.0049	—	.0015	-.0092	-.0131	-.0135	-.0128	-.0182	-.0212	-.0169
	.819	-.0206	-.0251	-.0274	-.0291	-.0324	-.0212	-.0214	-.0242	-.0315	-.0309
6.3	.137	.1116	.0829	.0634	.0351	.0204	.0045	.0054	.0056	.0094	.0148
	.546	.0129	—	.0039	-.0118	-.0216	-.0195	-.0197	-.0259	-.0304	-.0296
	.819	-.0212	-.0268	-.0309	-.0360	-.0433	-.0238	-.0249	-.0272	-.0405	-.0422
8.2	.137	.1324	.1005	.0756	.0371	.0189	.0045	.0047	.0028	.0060	.0080
	.546	.0306	—	.0111	-.0148	-.0311	-.0174	-.0186	-.0234	-.0300	-.0377
	.819	-.0101	-.0191	-.0296	-.0420	-.0506	-.0281	-.0283	-.0300	-.0420	-.0506

TABLE IV.- PRESSURE COEFFICIENT DATA FOR ELLIPTICAL BODY.
MAJOR AXIS HORIZONTAL

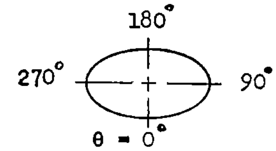

α, deg	Station x/L	Radial angle, θ, deg									
		0	315	290	280	270	90	100	110	135	180
0.1	0.137	.0244	.0294	.0377	.0394	.0447	.0396	.0356	.0377	.0317	.0294
	.546	−.0092	−.0088	−.0032	—	−.0069	−.0084	−.0062	−.0088	−.0111	−.0088
	.819	−.0210	−.0210	−.0219	−.0206	−.0171	−.0223	−.0238	−.0246	−.0244	−.0234
2.6	.137	.0450	.0506	.0529	.0519	.0409	.0261	.0214	.0208	.0141	.0133
	.546	−.0041	−.0077	−.0017	—	−.0184	−.0208	−.0169	−.0133	−.0124	−.0114
	.819	−.0270	−.0279	−.0334	−.0358	−.0210	−.0304	−.0266	−.0246	−.0227	−.0214
4.3	.137	.0630	.0683	.0602	.0533	.0225	.0073	.0034	.0101	.0062	.0064
	.546	.0146	.0051	−.0017	—	−.0304	−.0371	−.0287	−.0219	−.0169	−.0159
	.819	−.0223	−.0259	−.0426	−.0564	−.0354	−.0392	−.0362	−.0369	−.0255	−.0223
6.3	.137	.0877	.0895	.0731	.0553	.0004	−.0221	−.0330	−.0118	−.0092	−.0069
	.546	.0251	.0195	.0006	—	−.0692	−.0784	−.0467	−.0405	−.0304	−.0219
	.819	−.0096	−.0135	−.0467	−.0778	−.0456	−.0499	−.0504	−.0587	−.0328	−.0240
8.2	.137	.1112	.1099	.0904	.0611	−.0197	−.0418	−.0651	−.0302	−.0249	−.0096
	.546	.0476	.0399	.0090	—	−.0662	−.0806	−.0613	−.0645	−.0452	−.0251
	.819	.0047	−.0039	−.0409	−.0786	−.0495	−.0579	−.0587	−.0600	−.0581	−.0437

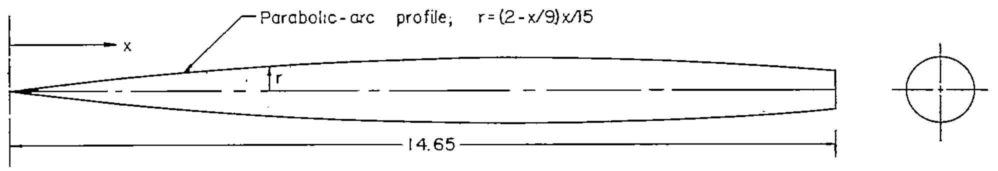

(a) RM-10 body.

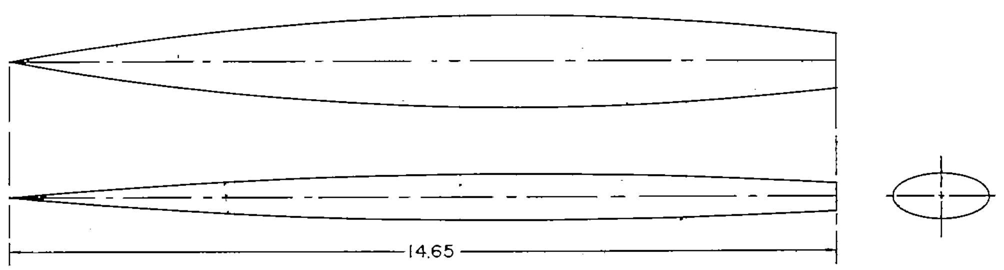

(b) Elliptical body.

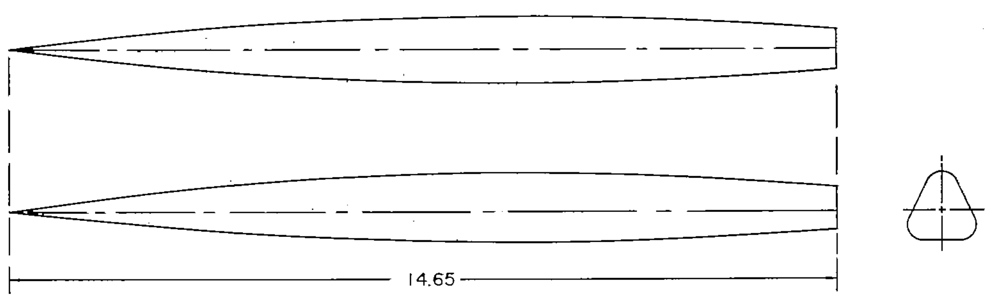

(c) Triangular body.

Figure 1.- General arrangement of bodies tested. All dimensions in inches.

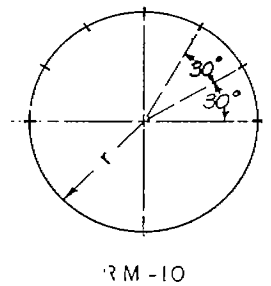

RM-10	
x	r
0	0
2	0.237
4	.415
6	.533
8	.5925
9	.600
10	.5925
12	.533
14	.415
14.65	.3635

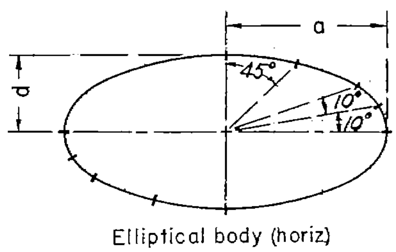

Elliptical		
x	a	d
0	0	0
2	0.335	0.1675
4	.587	.2935
6	.755	.3775
8	.838	.419
9	.849	.4245
10	.838	.419
12	.755	.3775
14	.587	.2935
14.65	.514	.257

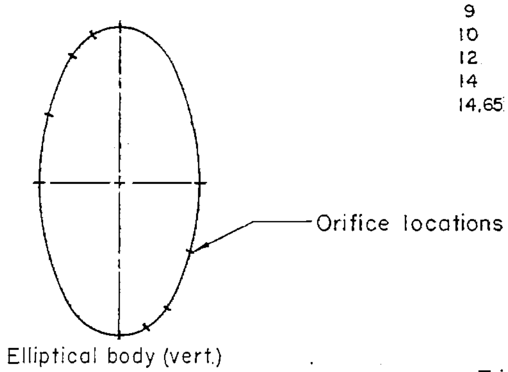

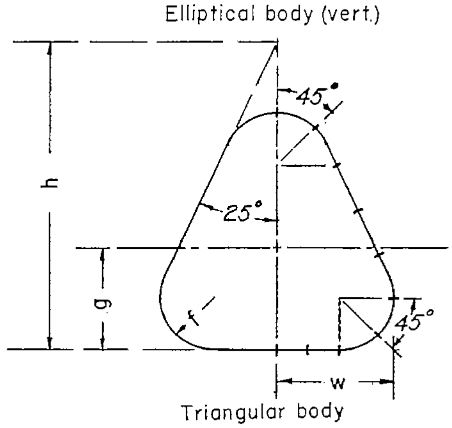

Triangular				
x	f	g	h	w
0	0	0	0	0
2	0.113	0.221	0.661	0.244
4	.198	.386	1.158	.427
6	.255	.496	1.488	.549
8	.283	.551	1.653	.610
9	.287	.558	1.674	.617
10	.283	.551	1.653	.610
12	.255	.496	1.488	.549
14	.198	.386	1.158	.427
14.65	.174	.338	1.014	.374

Figure 2.- Cross-section dimensions of bodies tested. All dimensions in inches.

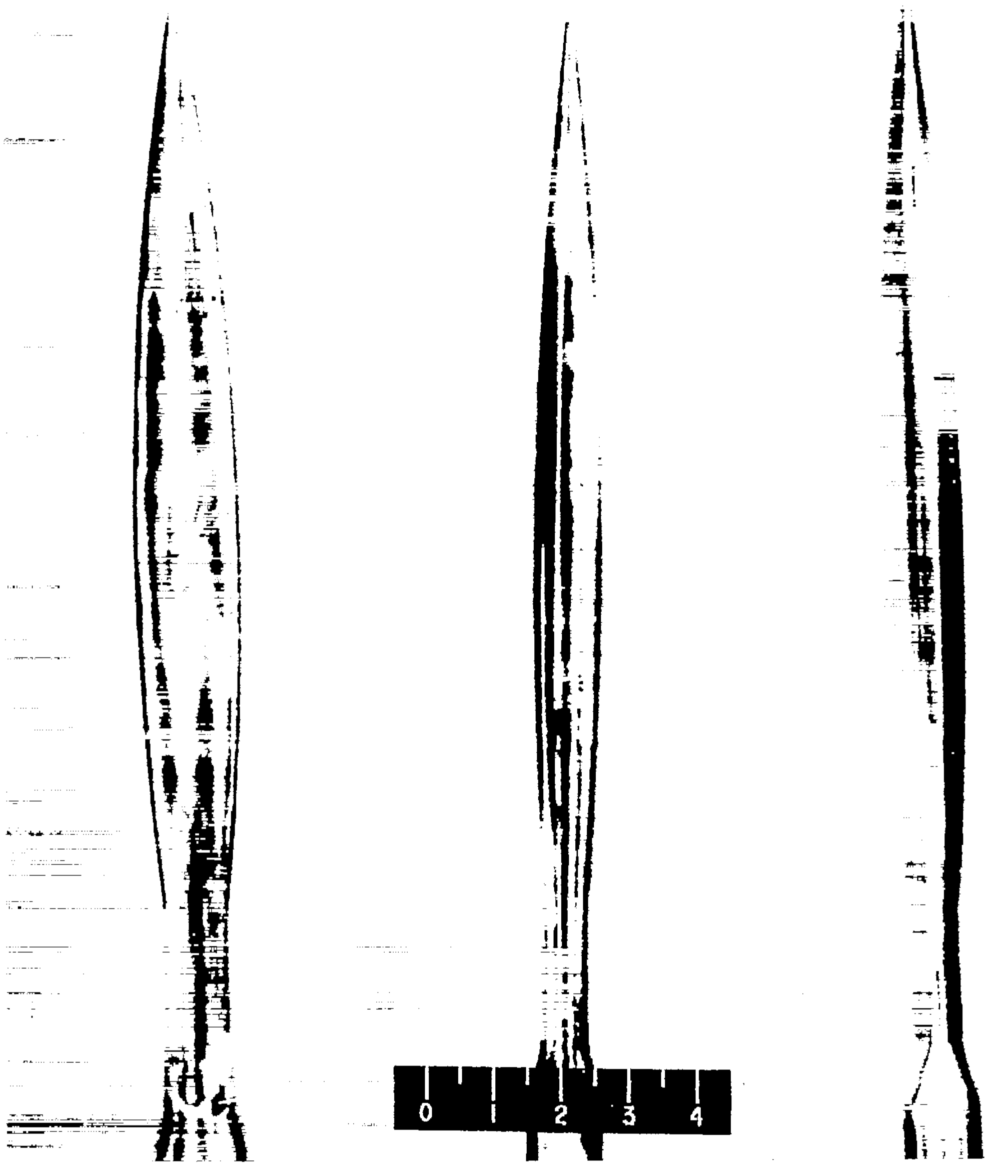

L-88854

(a) Plan view.

Figure 3.- Photographs of bodies used in pressure-distribution tests showing, from left to right, the elliptical-, circular-, and triangular-cross-section bodies.

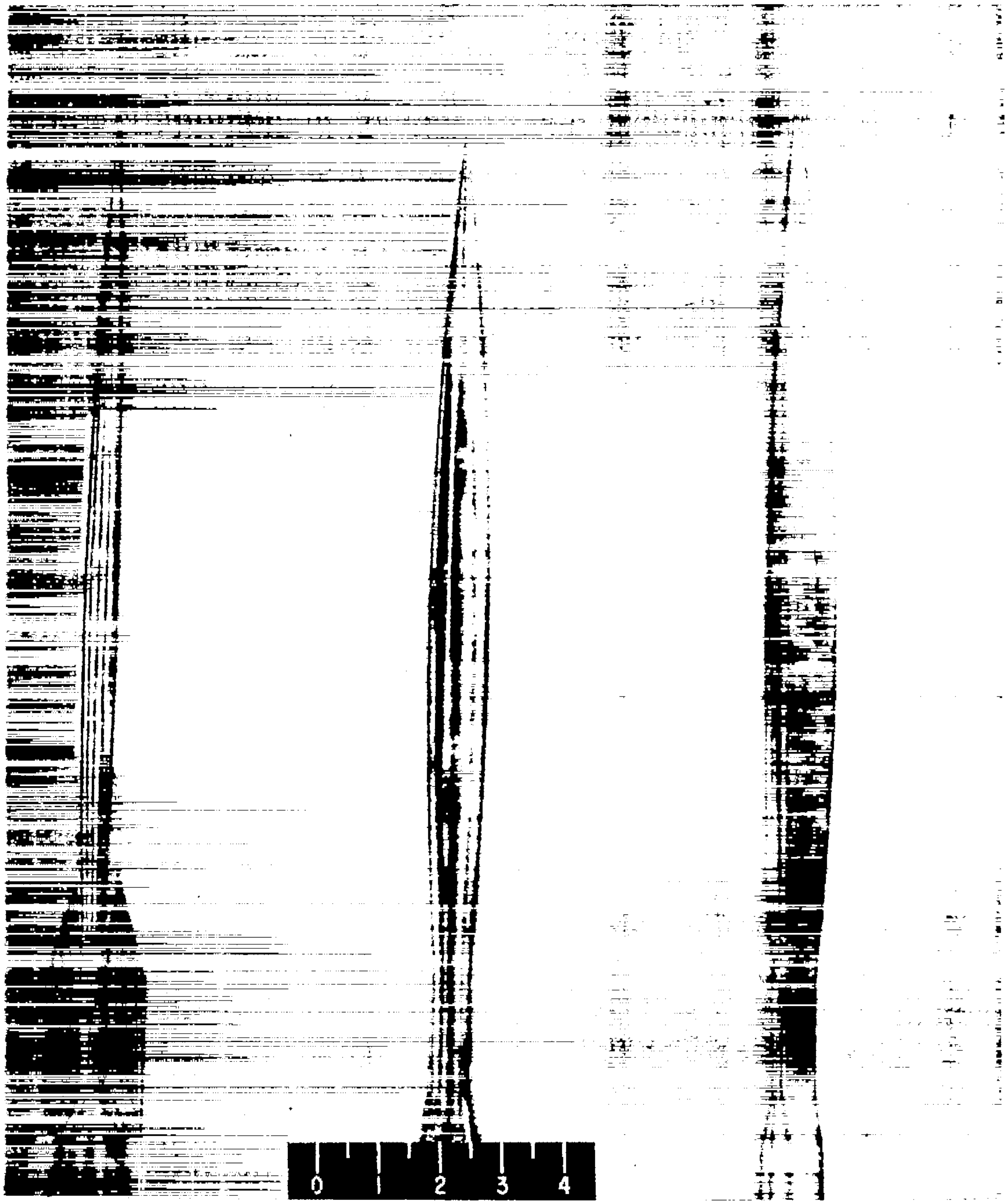

L-88855

(b) Side view.

Figure 3.- Concluded.

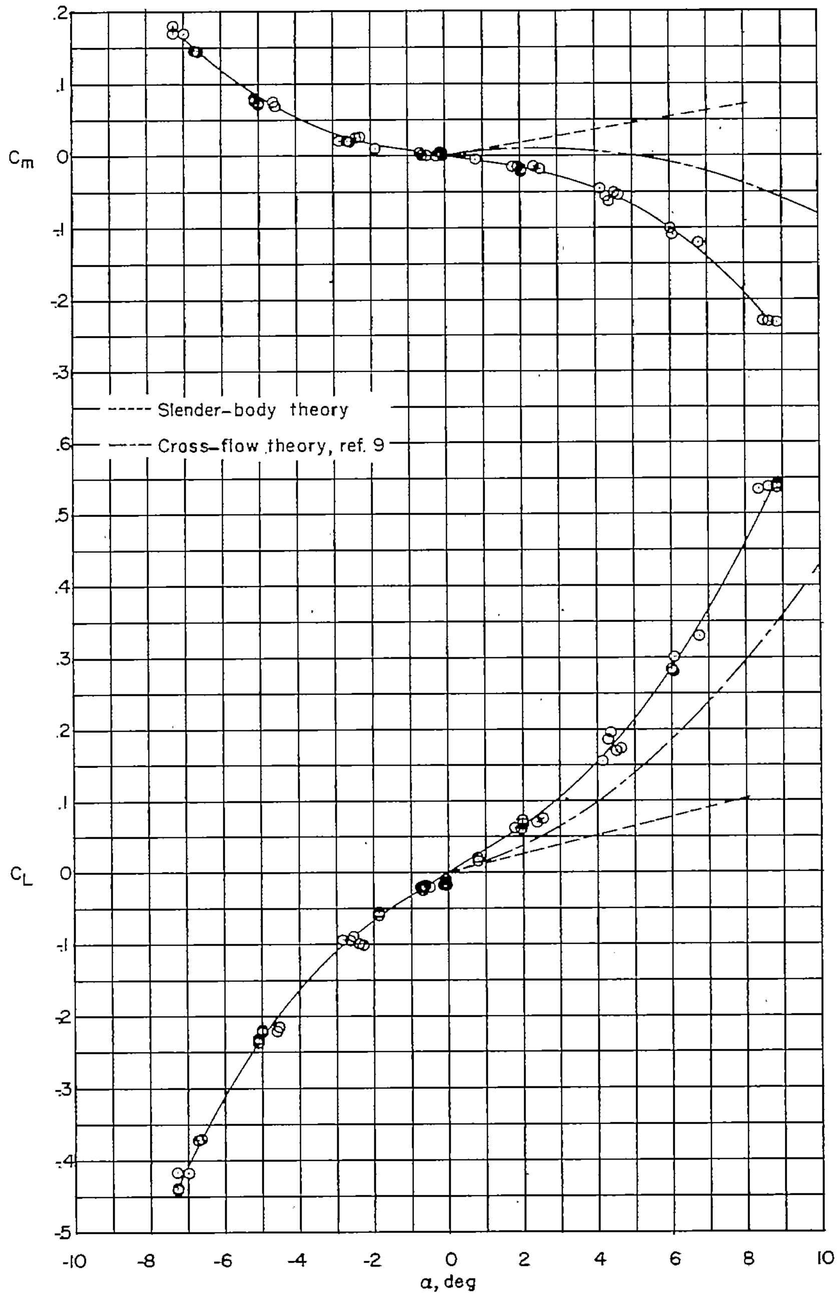

(a) Variation of C_L and C_m with α.

Figure 4.- Force measurements of NACA RM-10 body. $M = 3.12$; $R = 29 \times 10^6$.

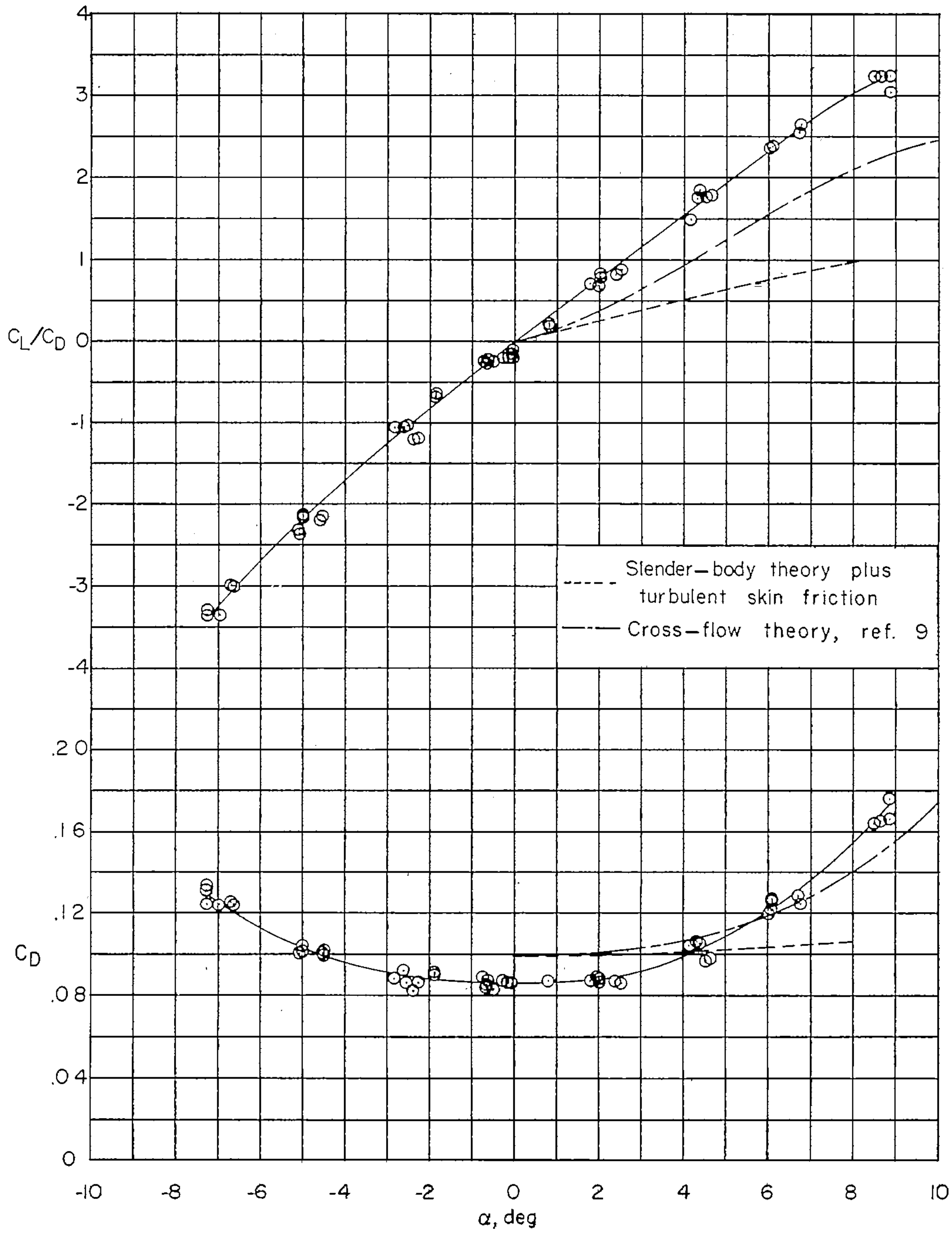

(b) Variation of C_D and C_L/C_D with α.

Figure 4.- Concluded.

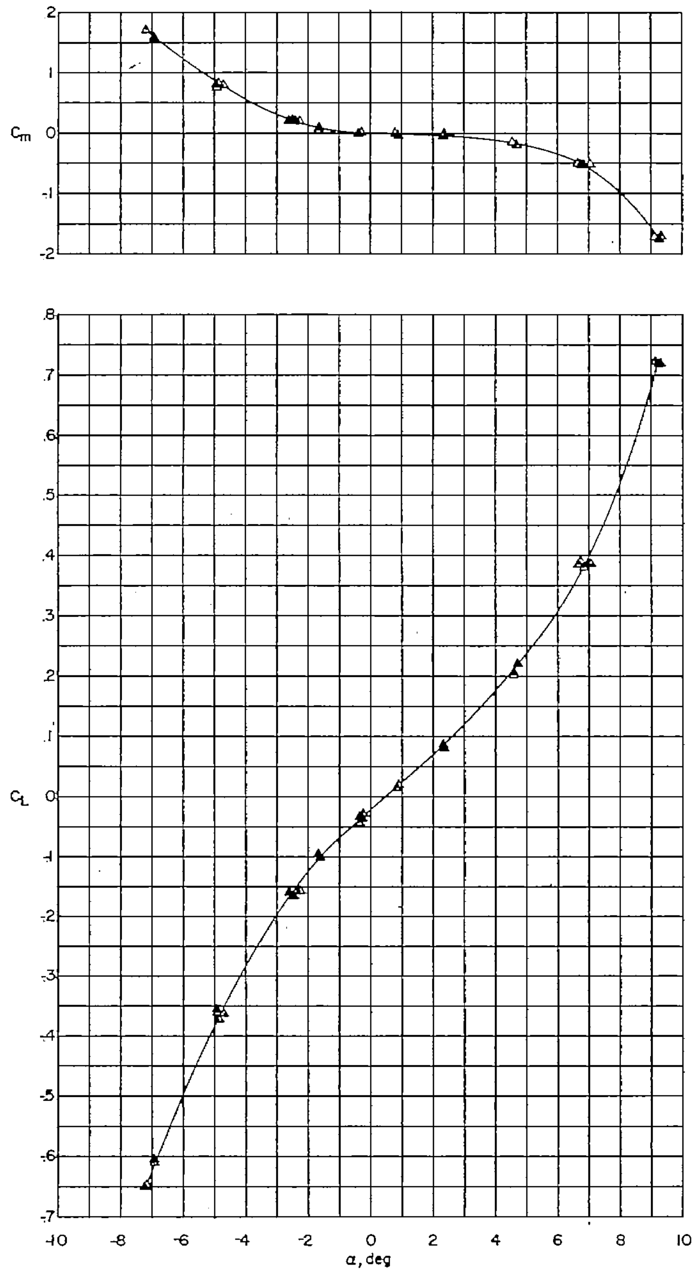

(a) Variation of C_L and C_m with α.

Figure 5.- Force measurements of triangular body. $M = 3.12$; $R = 33 \times 10^6$.

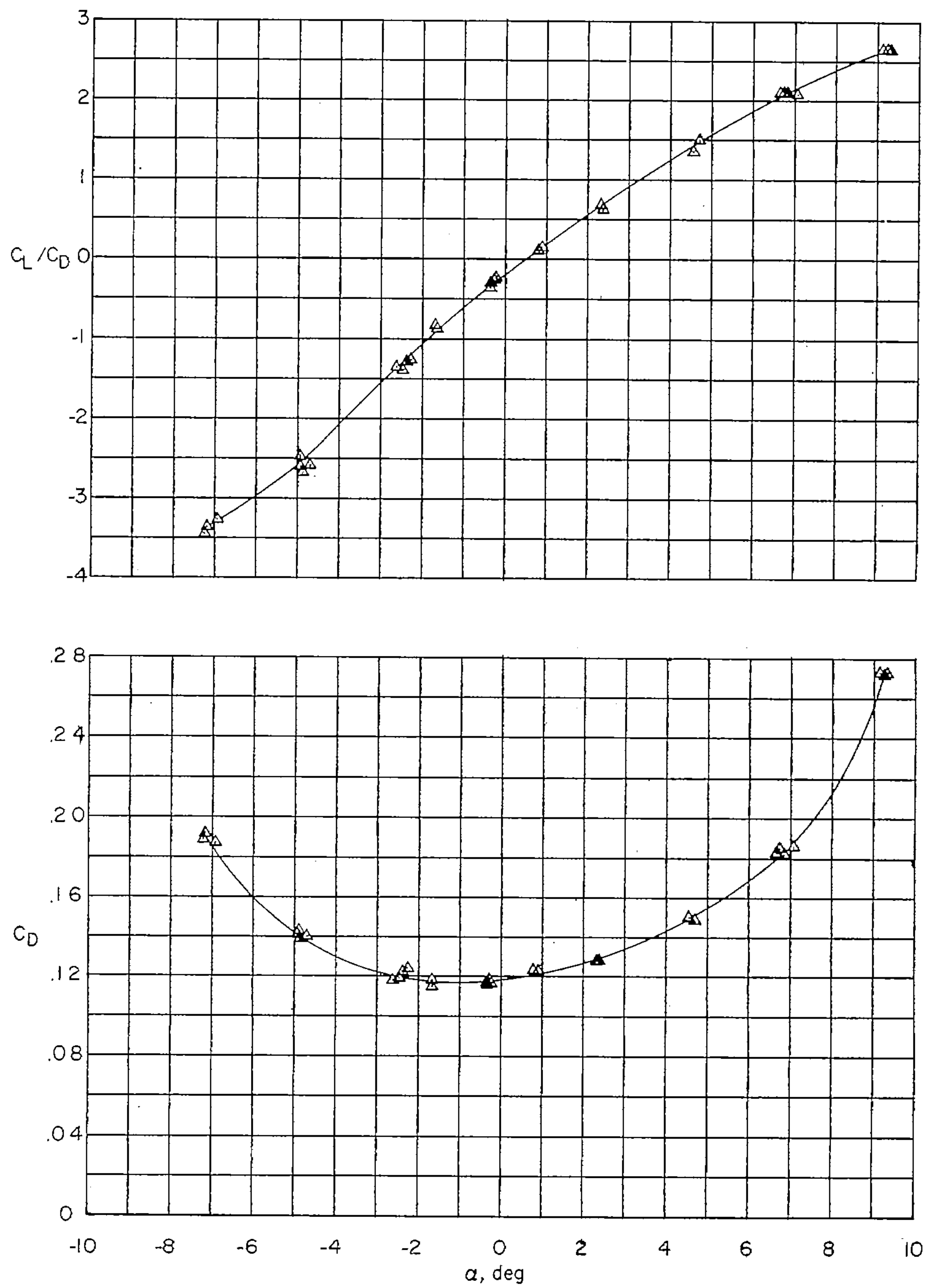

(b) Variation of C_D and C_L/C_D with α.

Figure 5.- Concluded.

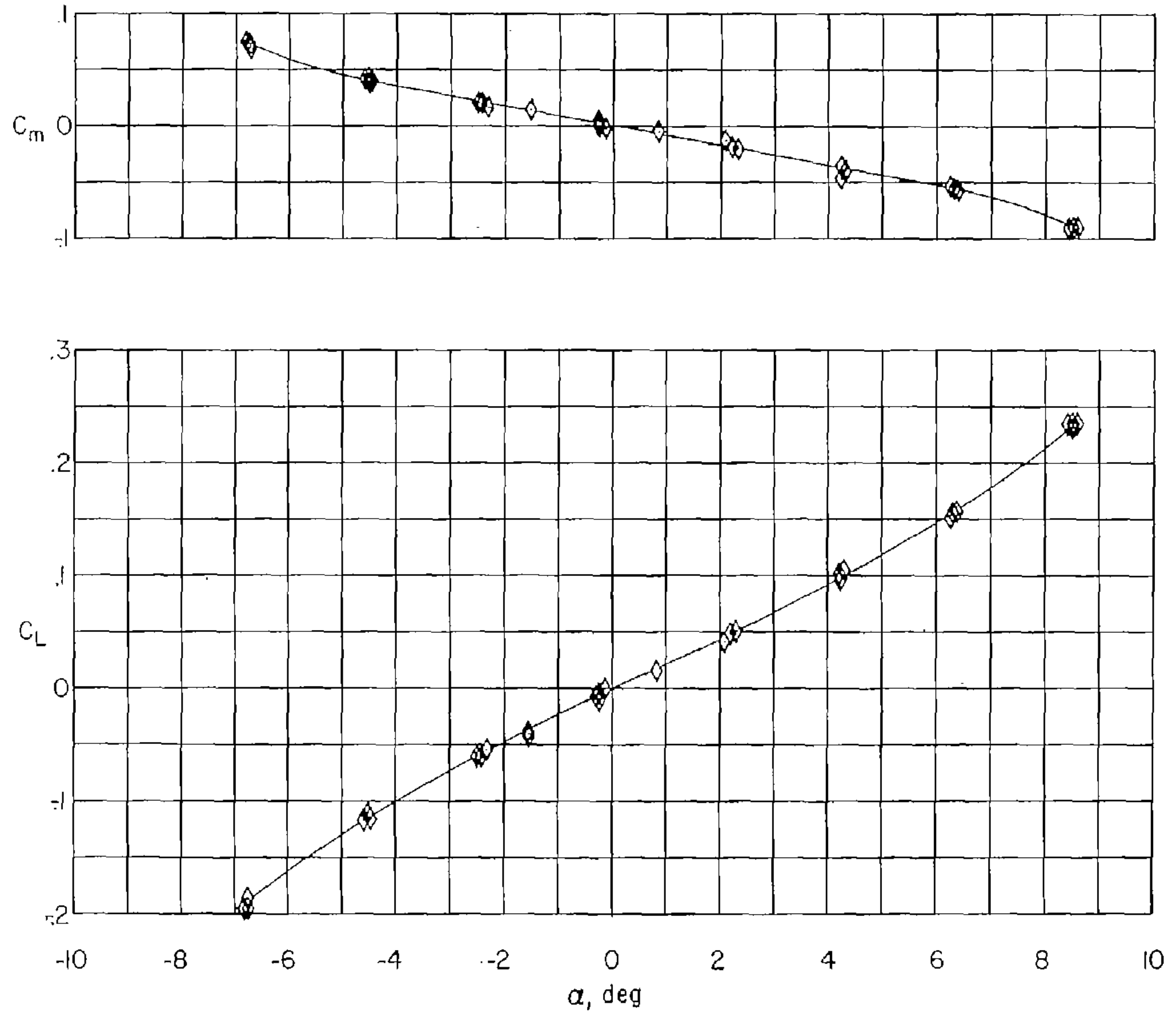

(a) Variation of C_L and C_m with α.

Figure 6.- Force measurements of elliptical body with major axis vertical. $M = 3.12$; $R = 29 \times 10^6$.

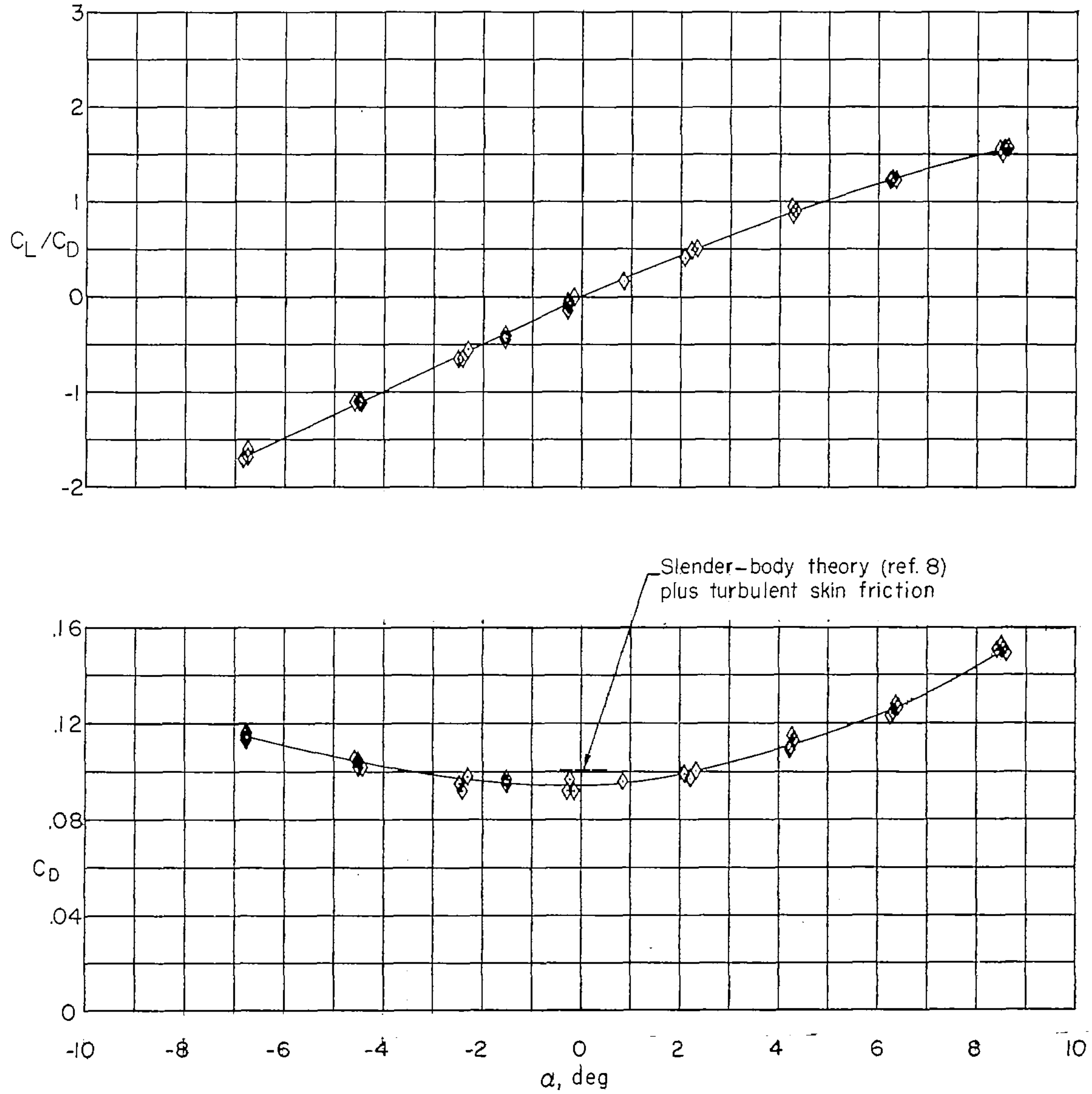

(b) Variation of C_D and C_L/C_D with α.

Figure 6.- Concluded.

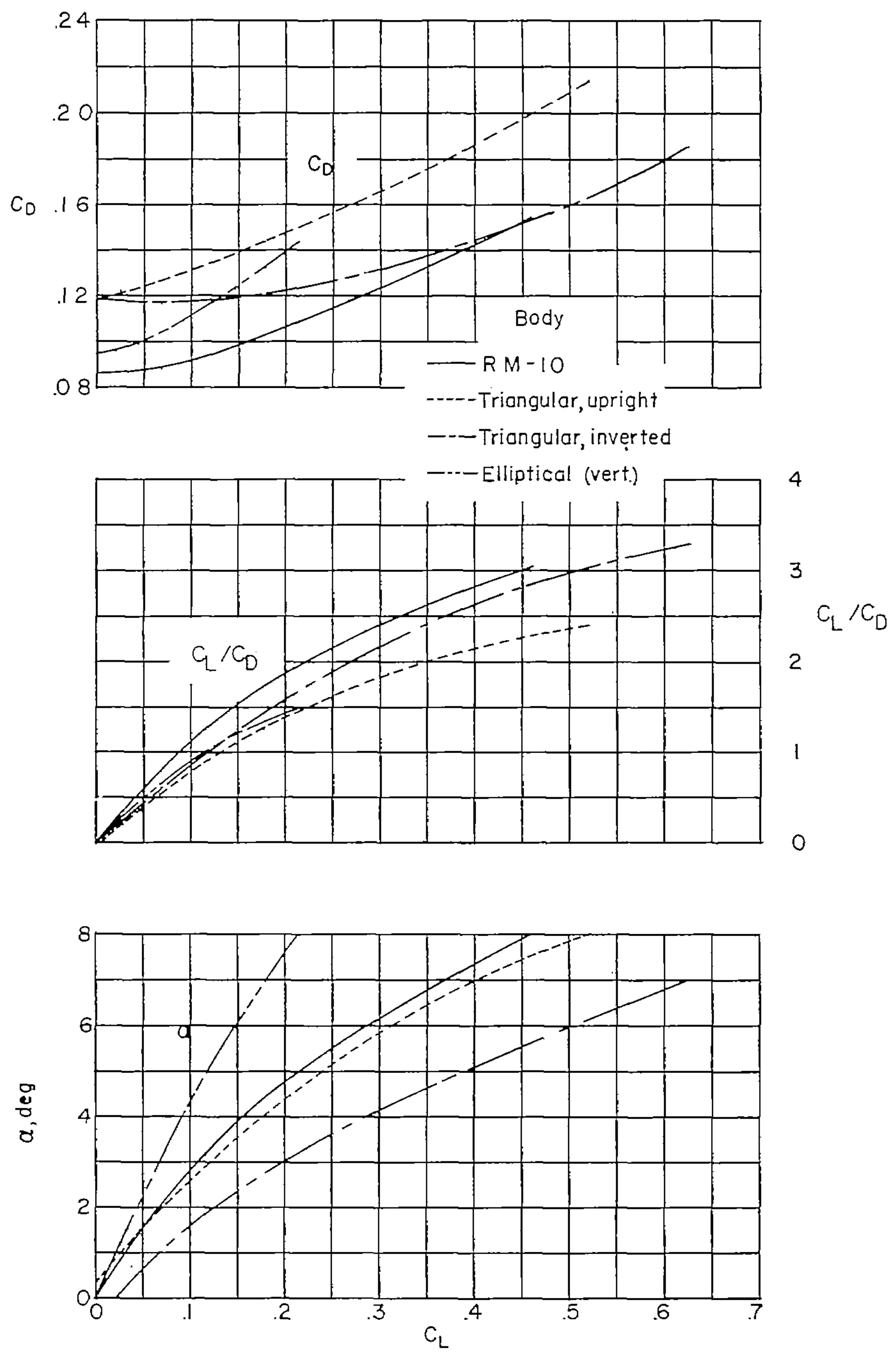

Figure 7.- Variation of α, C_L/C_D, and C_D with C_L for four body configurations. $M = 3.12$.

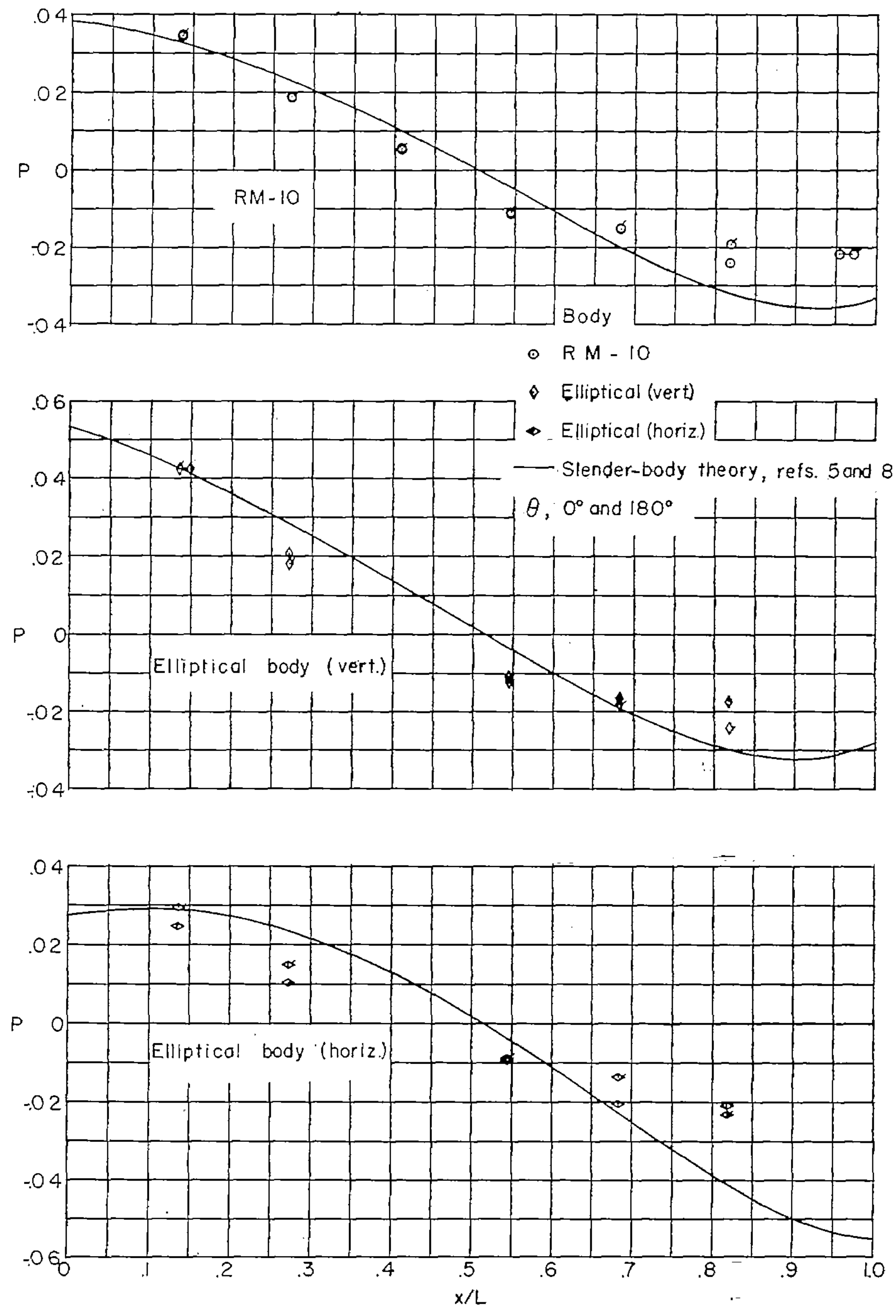

Figure 8.- Variation of pressure coefficient with longitudinal position along body for three body configurations. $\alpha_N = 0^\circ$; flagged symbols denote pressure coefficients at $\theta = 180^\circ$; $M = 3.12$.

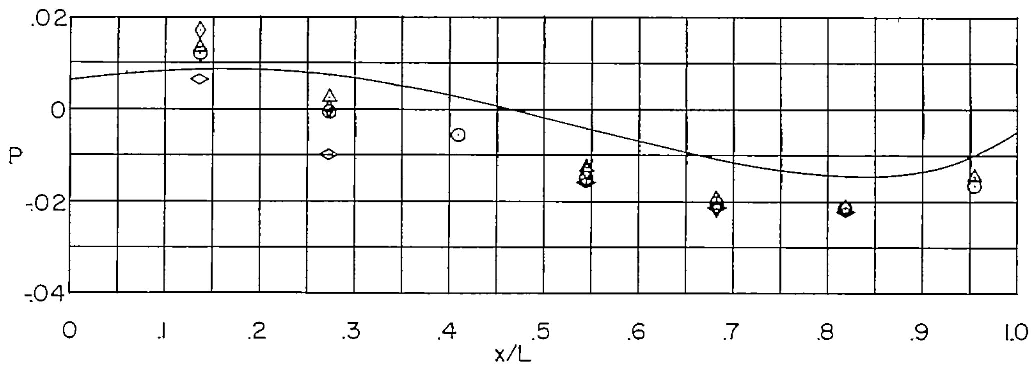

(a) Leeward side; $\theta = 80^{\circ}$.

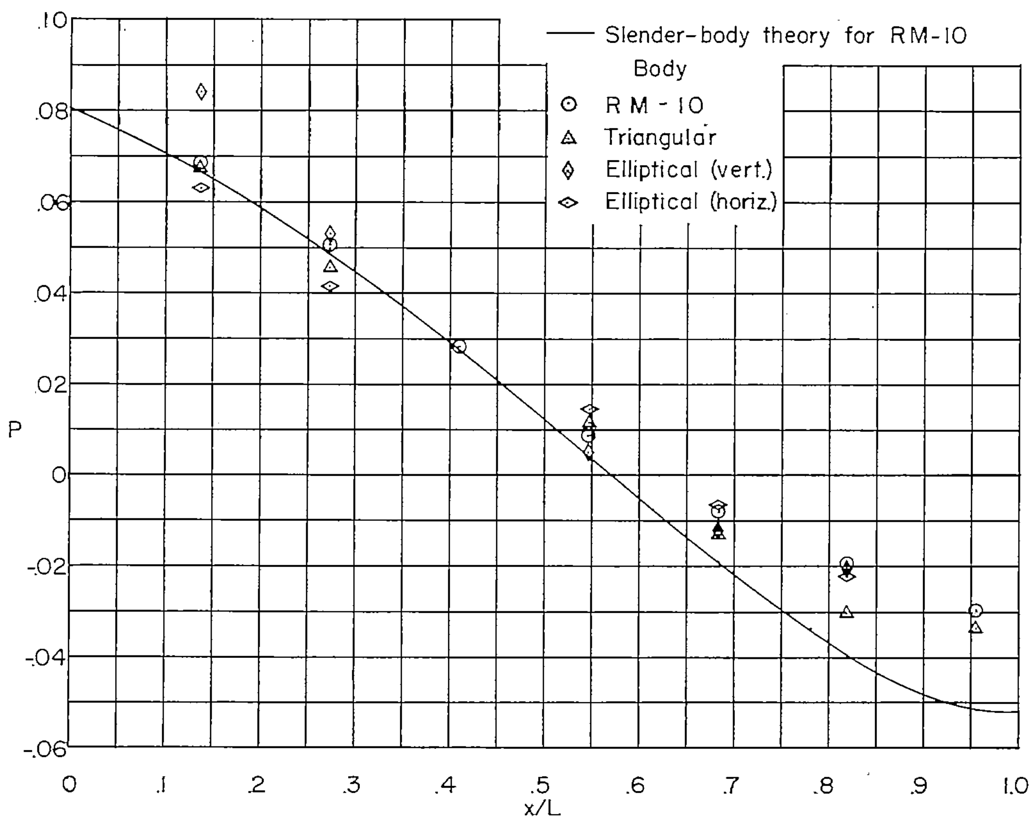

(b) Windward side; $\theta = 0^{\circ}$.

Figure 9.- Variation of pressure coefficient with longitudinal position along body for four body configurations. $\alpha_N = 4^{\circ}$; $M = 3.12$.

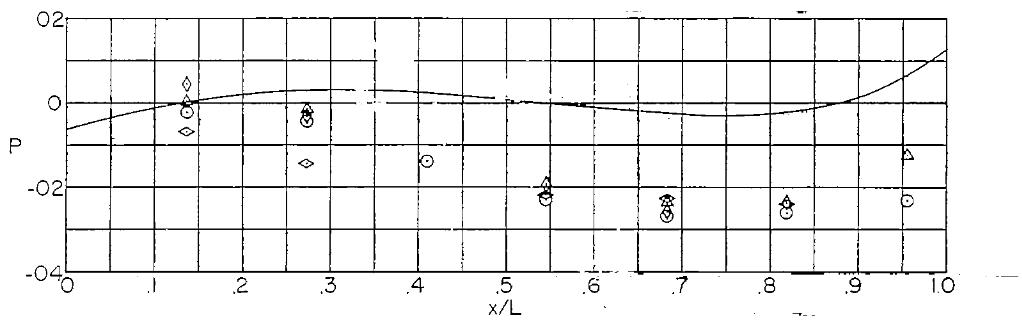

(a) Leeward side; $\theta = 180^\circ$.

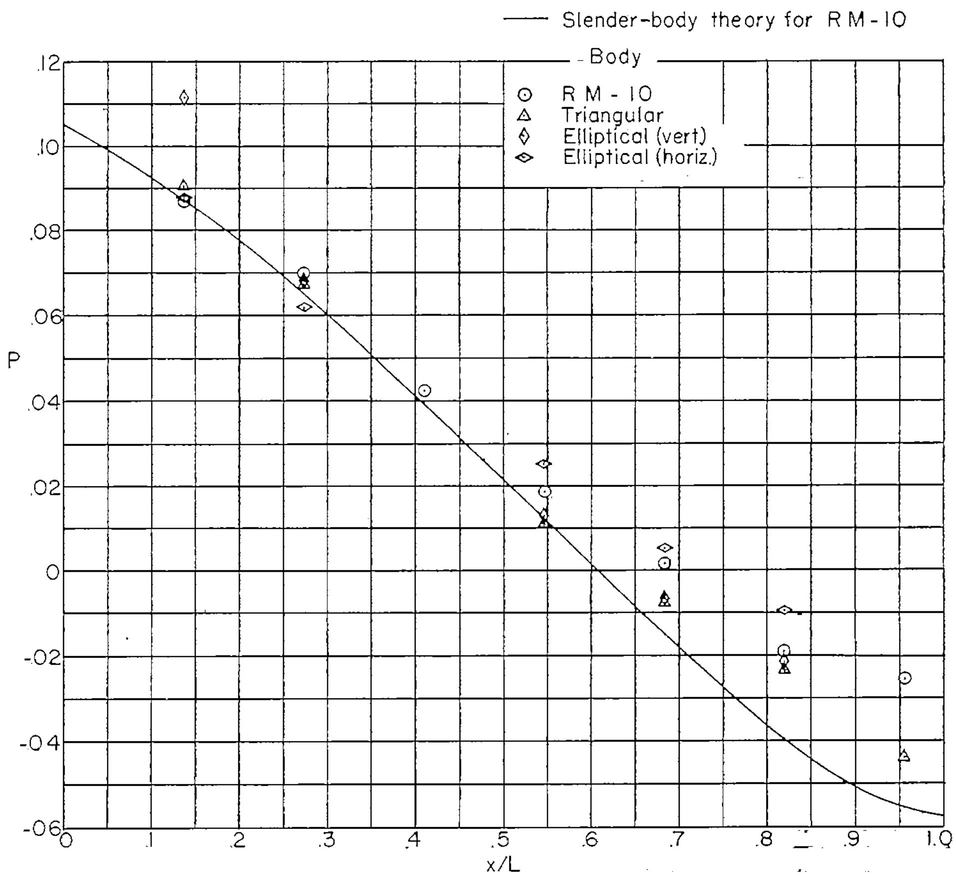

(b) Windward side; $\theta = 0^\circ$.

Figure 10.- Variation of pressure coefficient with longitudinal position along body for four body configurations. $\alpha_N = 6^\circ$; M = 3.12.

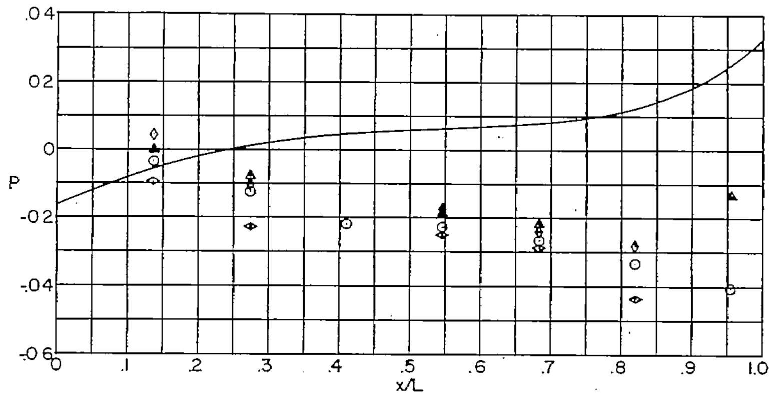

(a) Leeward side; $\theta = 180^{\circ}$.

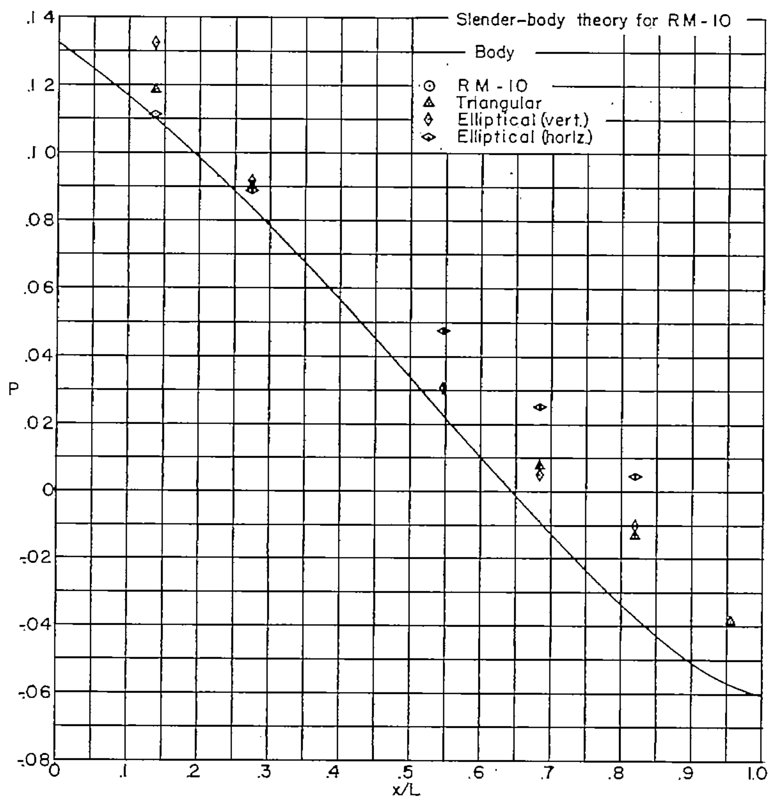

(b) Windward side; $\theta = 0^{\circ}$.

Figure 11.- Variation of pressure coefficient with longitudinal position along body for four body configurations. $\alpha_N = 8^{\circ}$; $M = 3.12$.

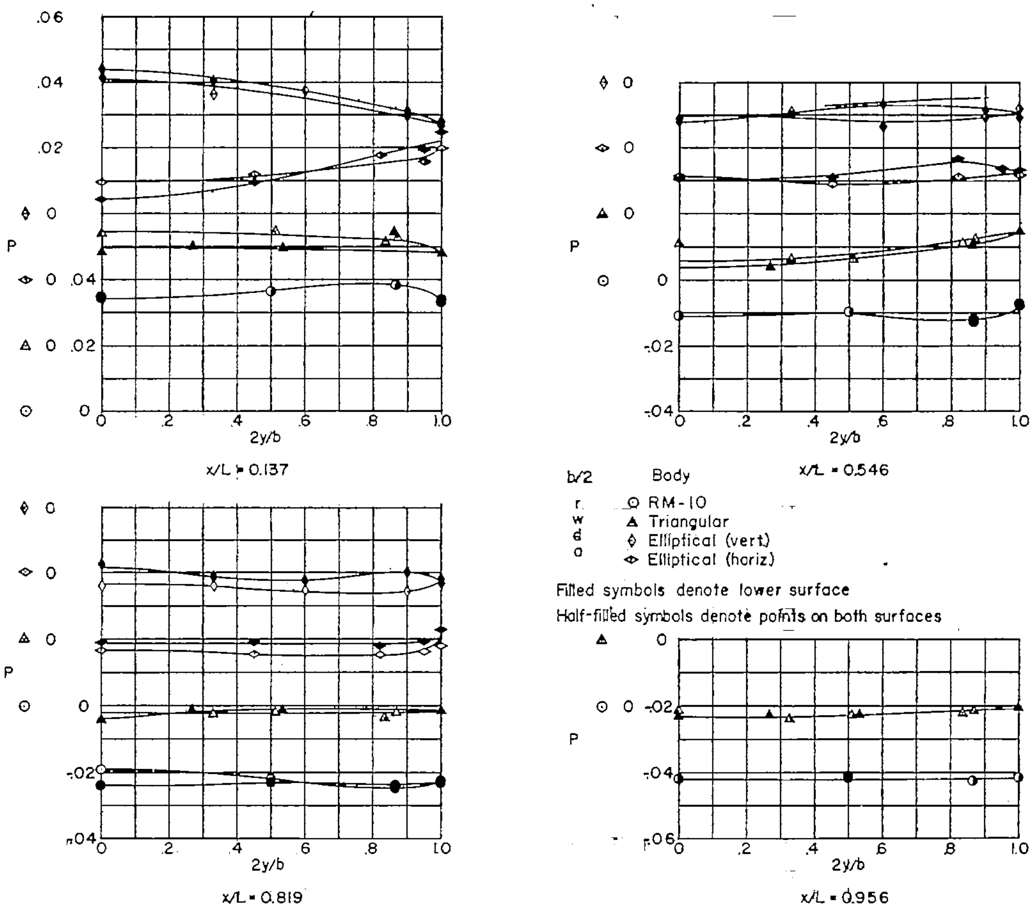

(a) $\alpha_N = 0^\circ$.

Figure 12.- Variation of pressure coefficient with body width about the plane of symmetry for four longitudinal locations. $M = 3.12$; $R = 29 \times 10^6$.

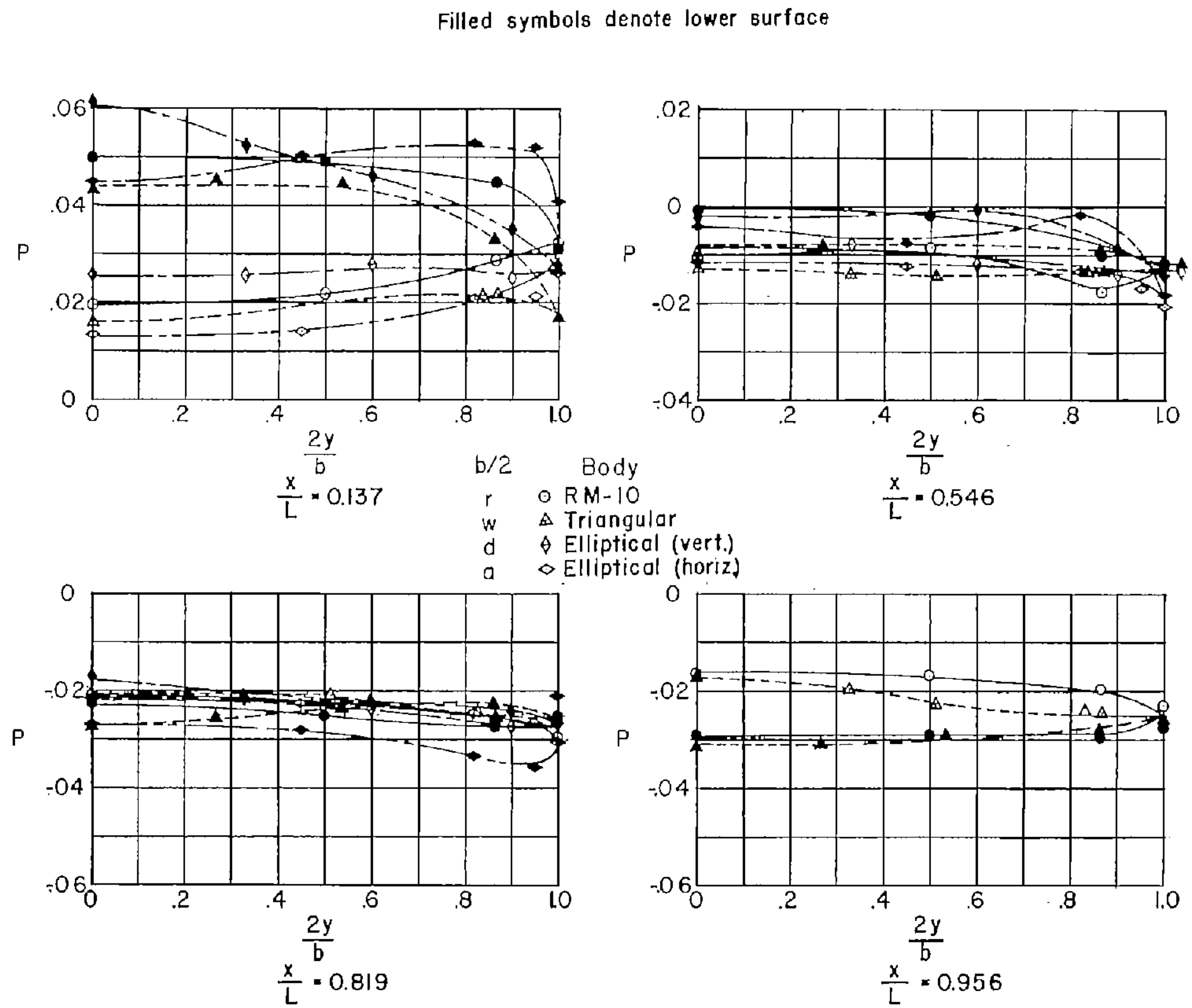

(b) $\alpha_N = 2^{\circ}$.

Figure 12.- Continued.

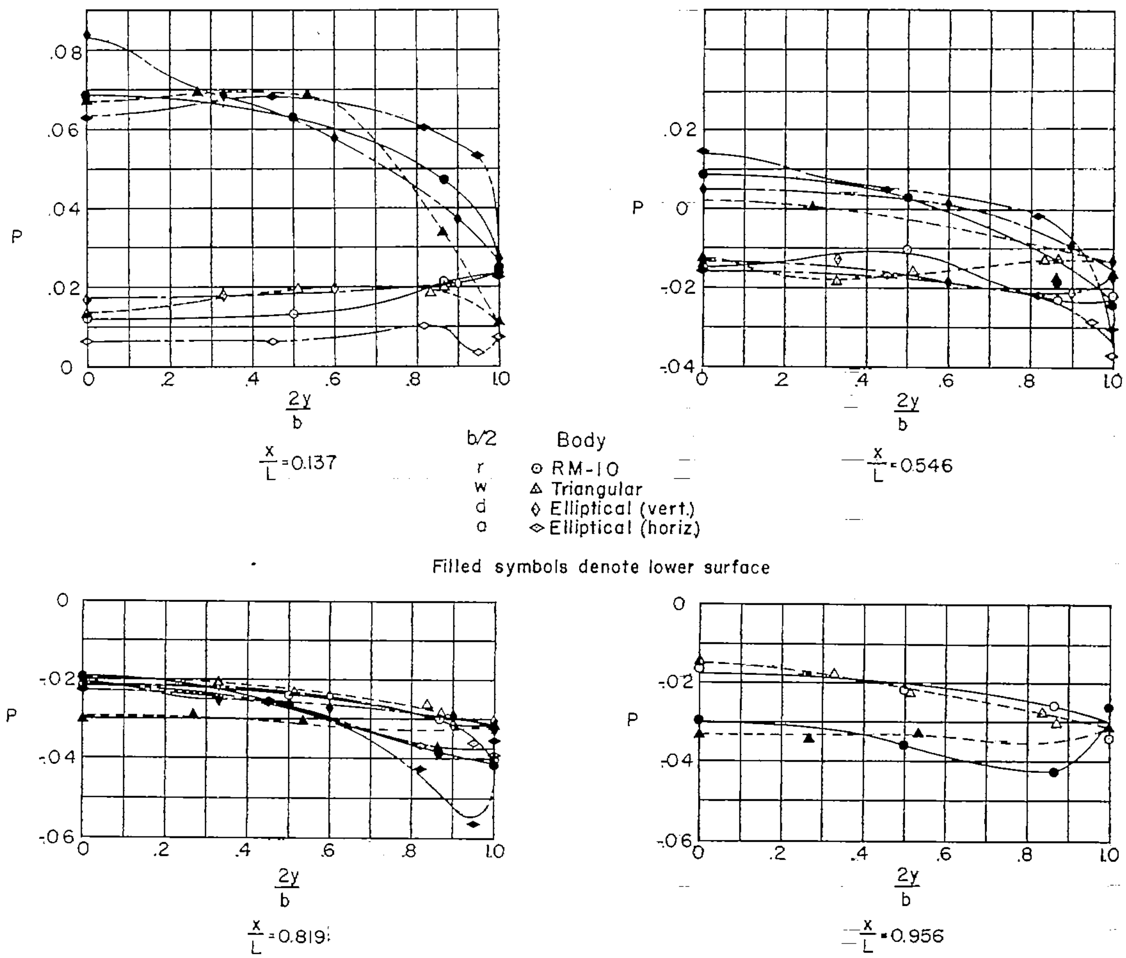

(c) $\alpha_N = 4^{\circ}$.

Figure 12.- Continued.

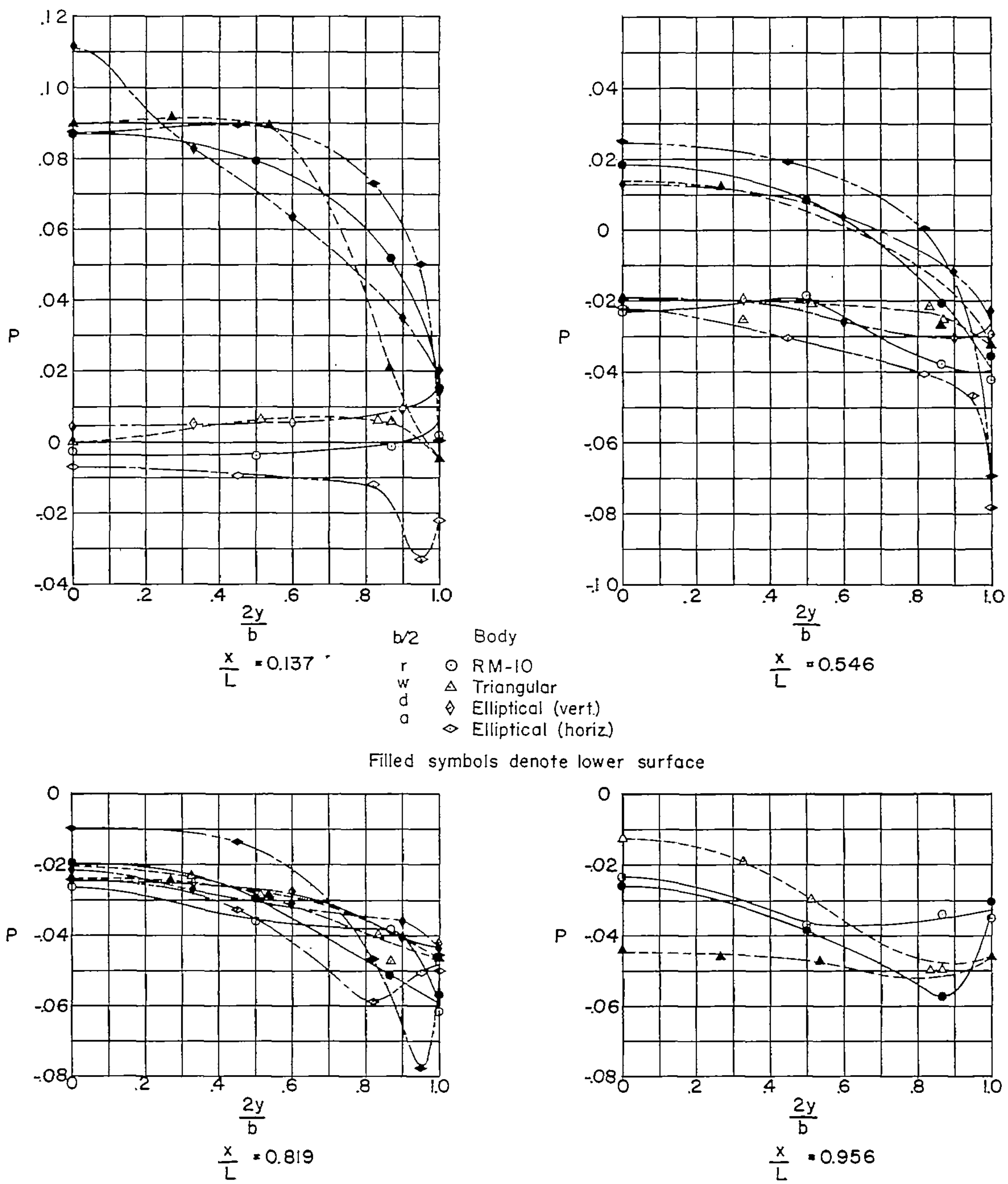

(d) $\alpha_N = 6^{\circ}$.

Figure 12.- Continued.

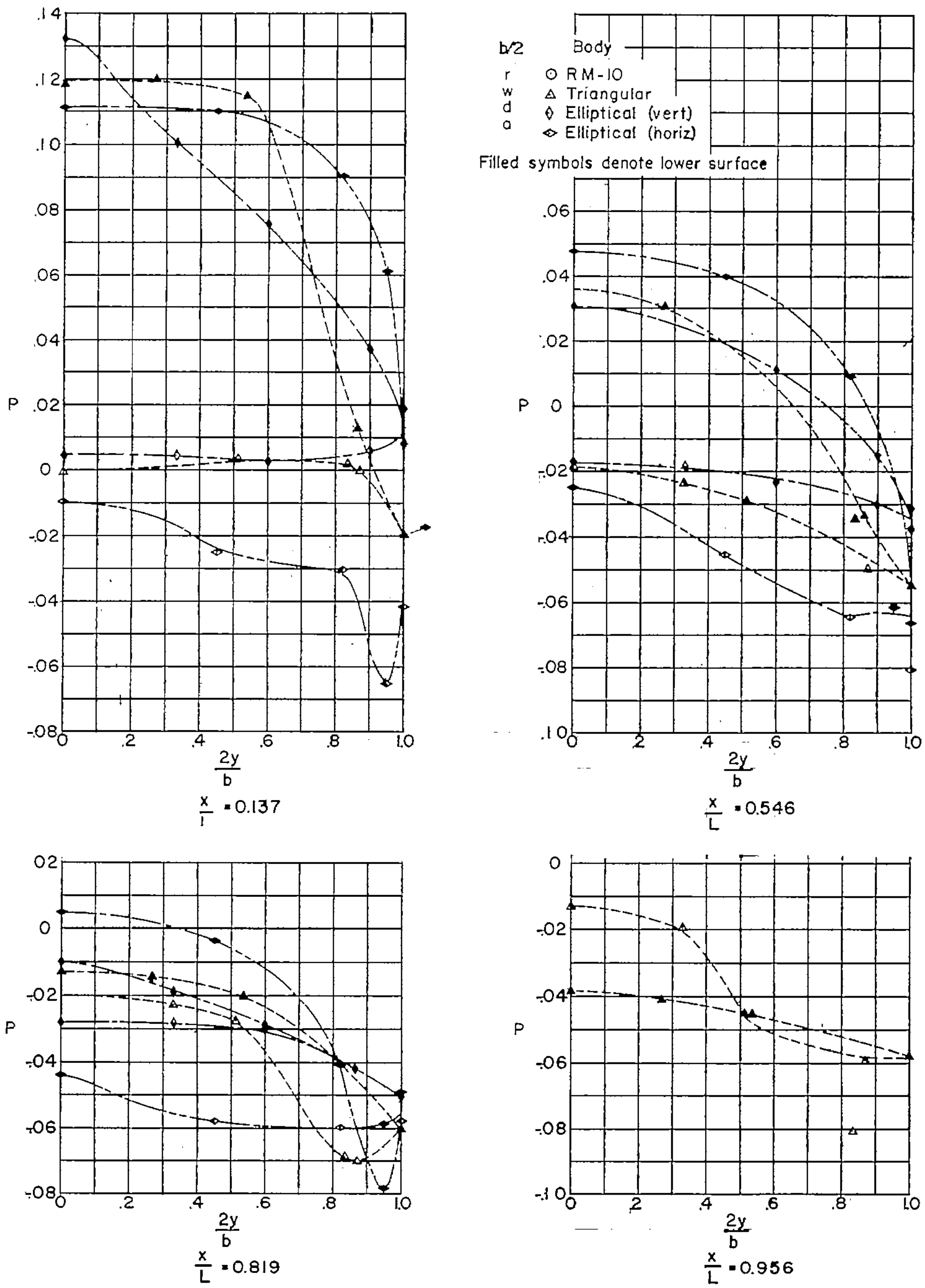

(e) $\alpha_N = 8^{\circ}$.

Figure 12.- Concluded.

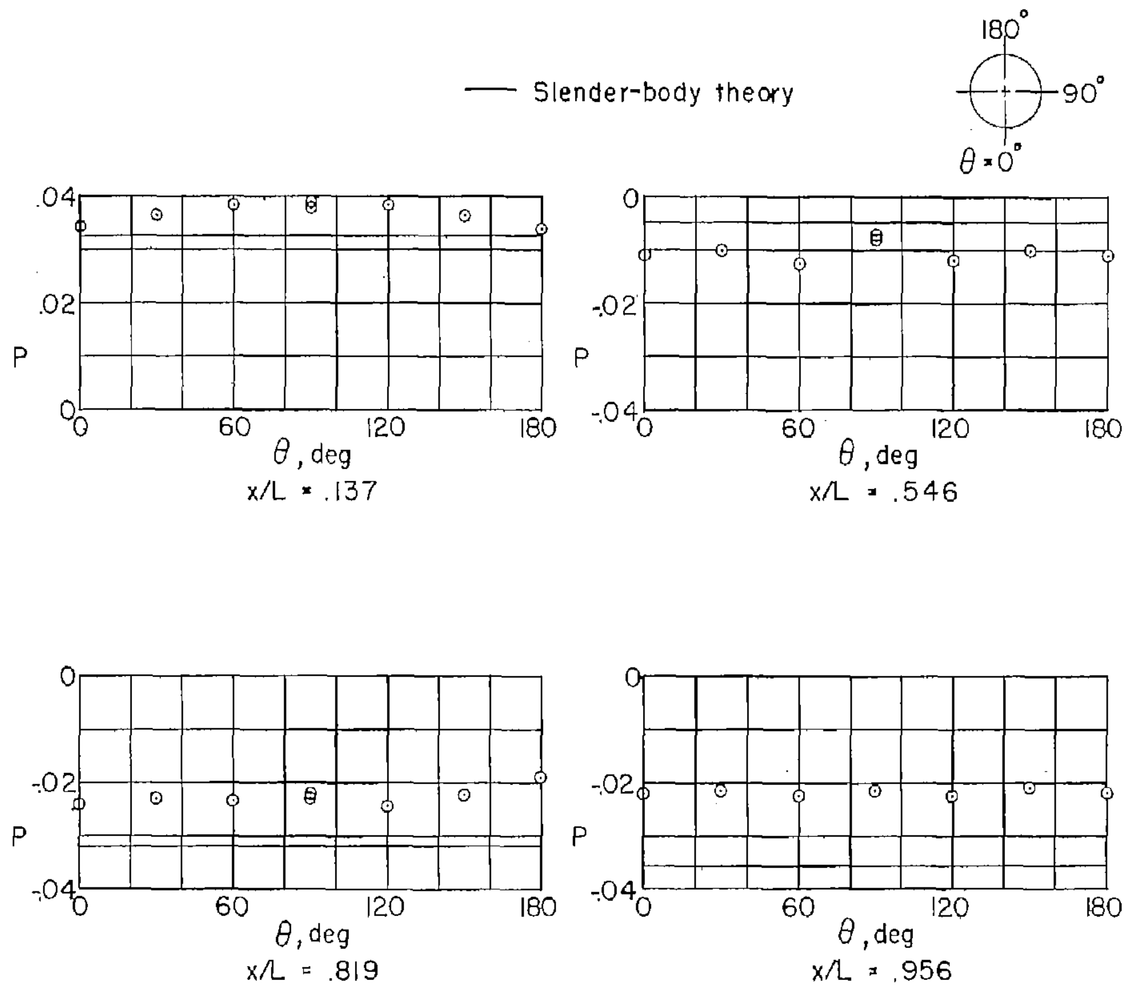

(a) $\alpha_N = 0^{\circ}$.

Figure 13.- Variation of pressure coefficient with radial position for four longitudinal locations on the NACA RM-10 body. $M = 3.12$.

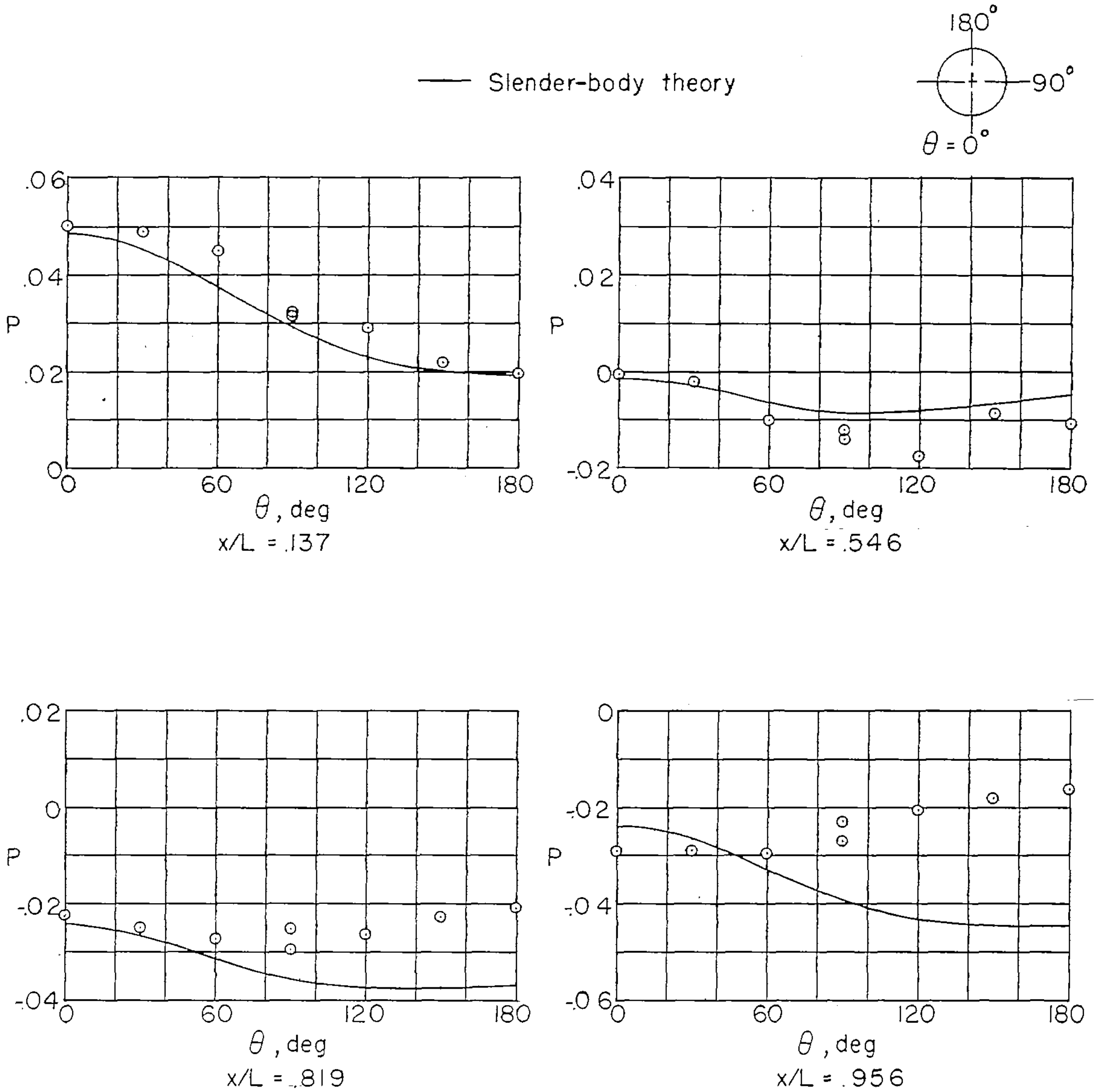

(b) $\alpha_N = 2^{\circ}$.

Figure 13.- Continued.

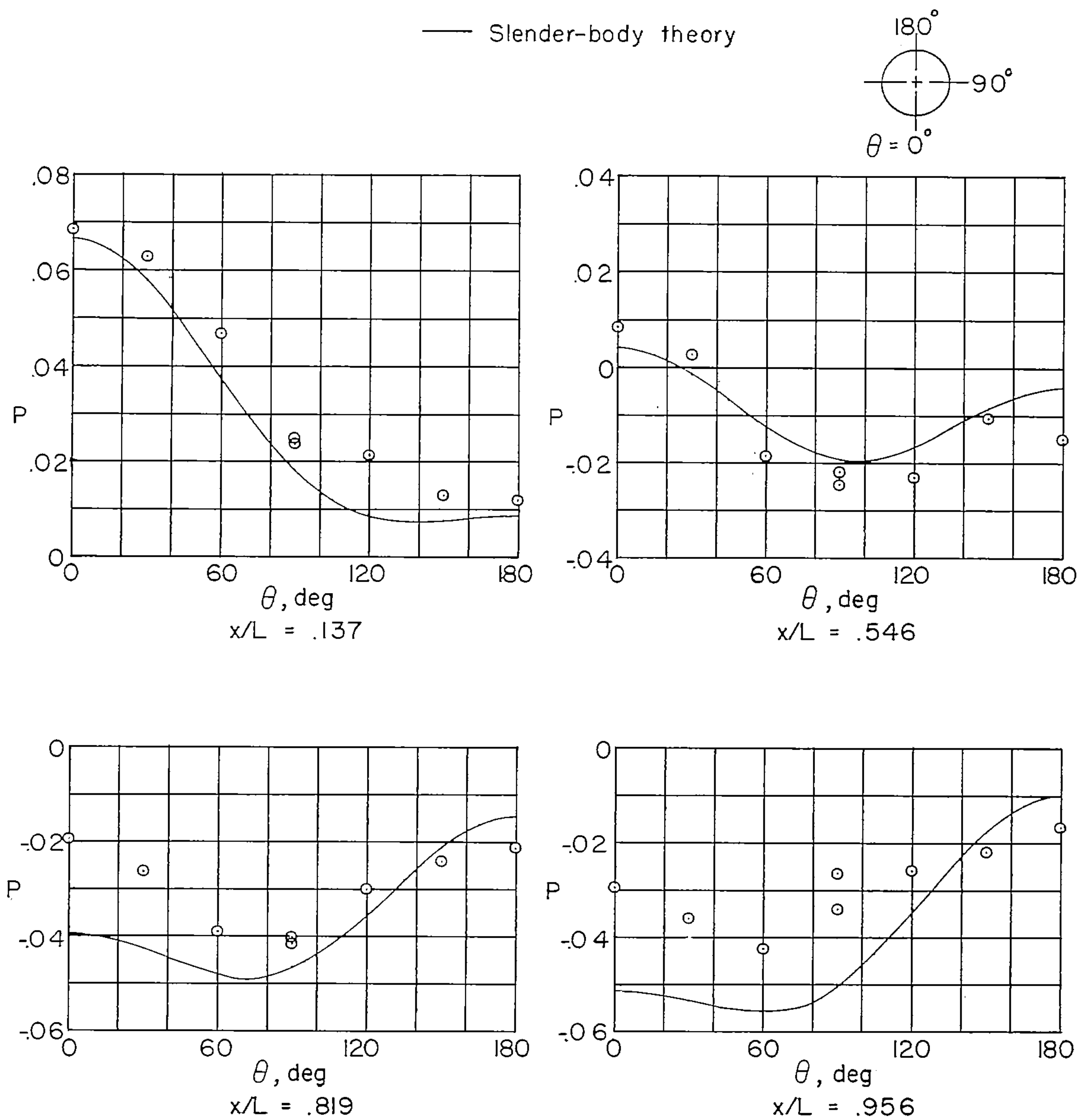

(c) $\alpha_N = 4^{\circ}$.

Figure 13.- Continued.

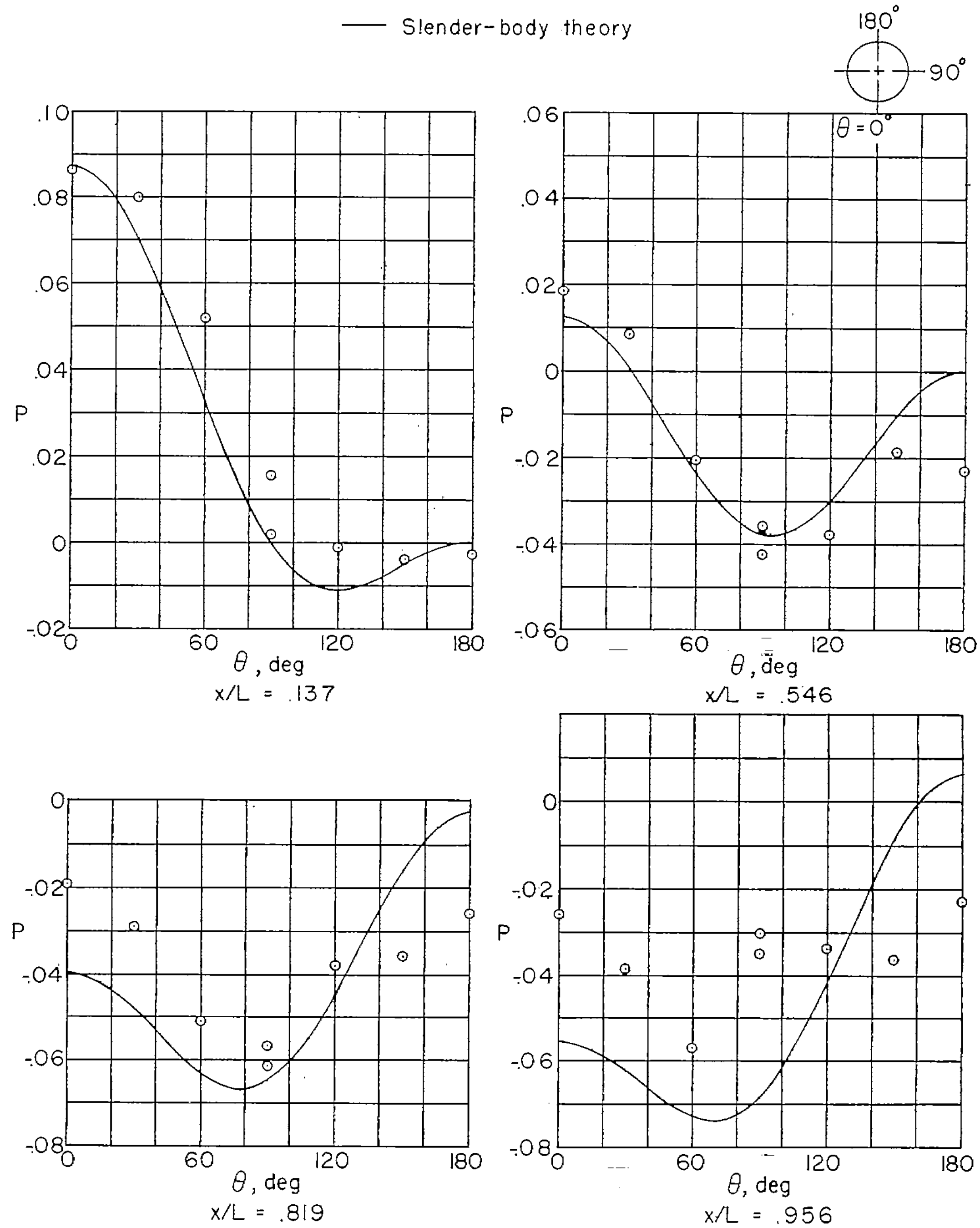

(d) $\alpha_N = 6^{\circ}$.

Figure 13.- Concluded.

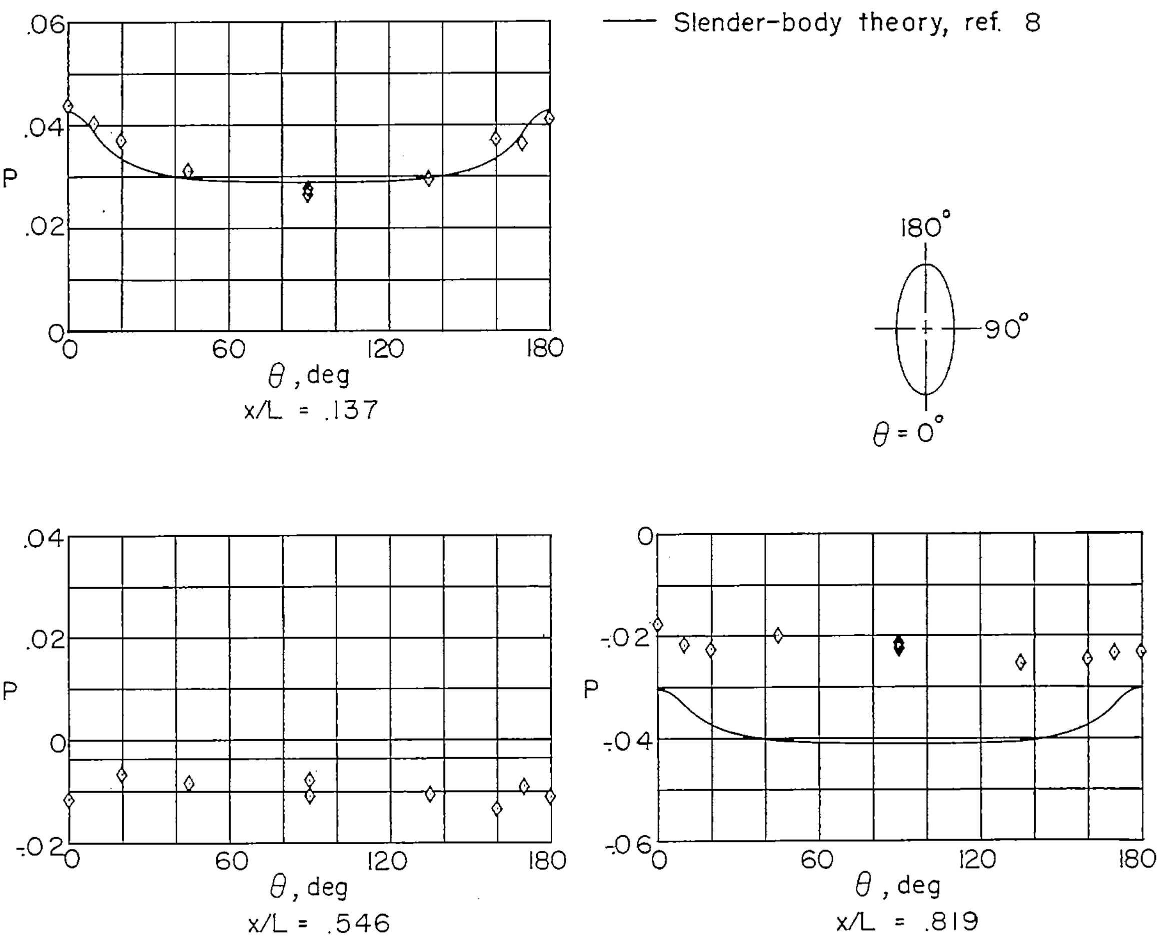

(a) Elliptical body (major axis vertical).

Figure 14.- Variation of pressure coefficient with radial position for three longitudinal locations on the elliptical body. $\alpha_N = 0^\circ$; $M = 3.12$.

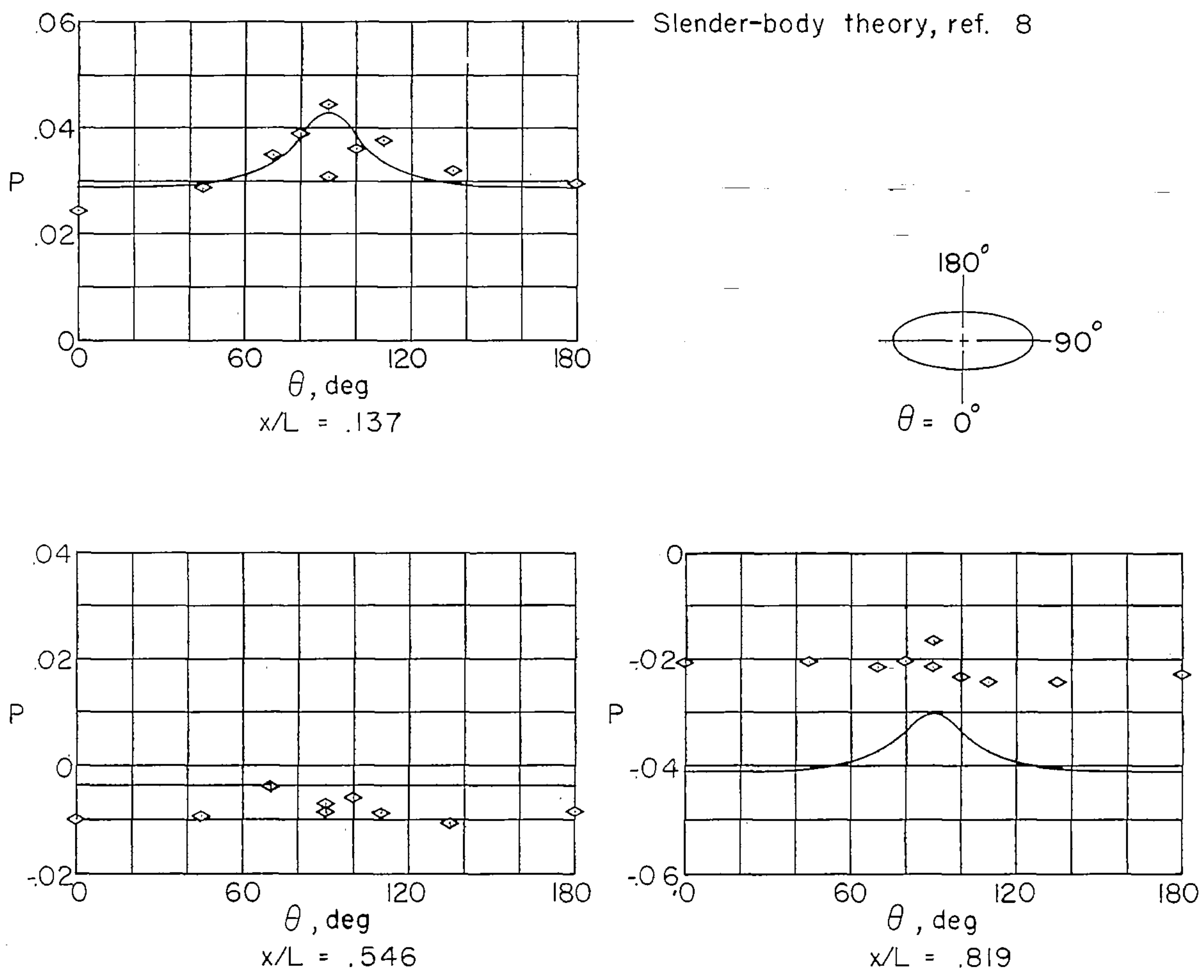

(b) Elliptical body (major axis horizontal).

Figure 14.- Concluded.

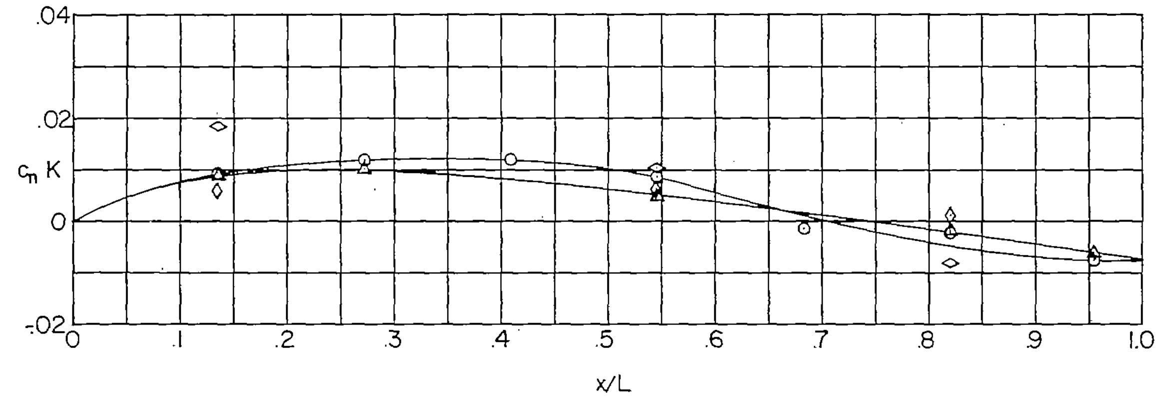

(a) $\alpha_N = 2^\circ$.

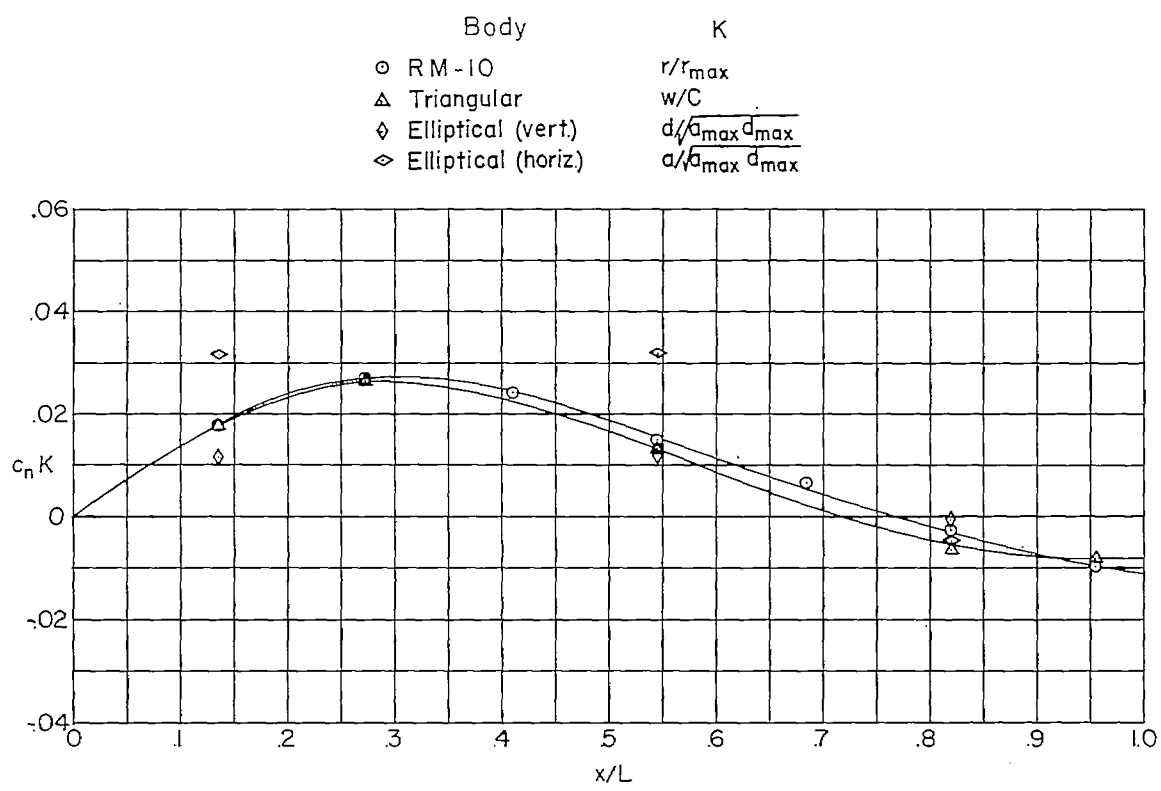

(b) $\alpha_N = 4^\circ$.

Figure 15.- Variation of section loading parameter with longitudinal location for four body configurations. M = 3.12.

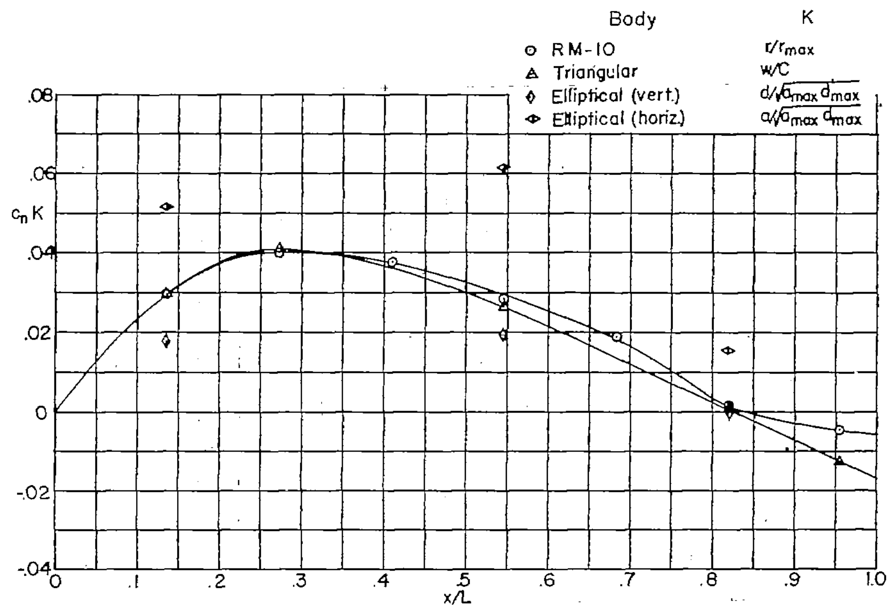

(c) $\alpha_N = 6^\circ$.

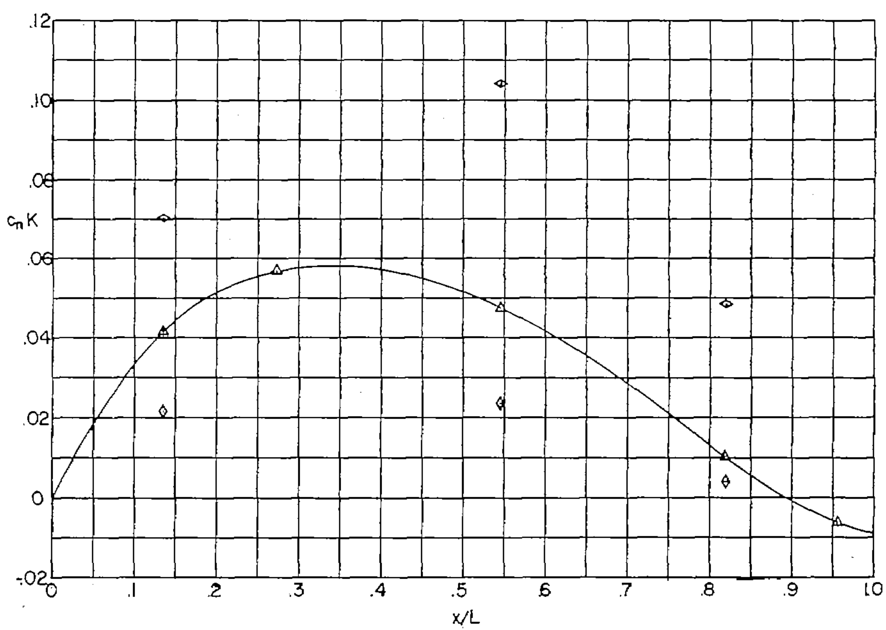

(d) $\alpha_N = 8^\circ$.

Figure 15.- Concluded.

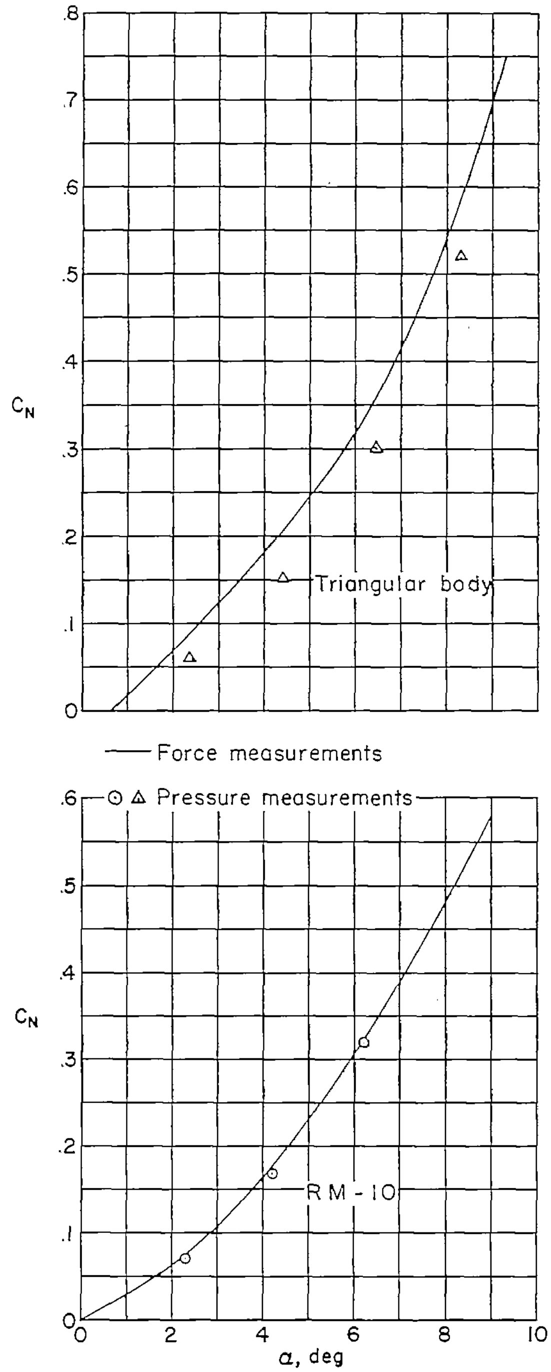

Figure 16.- Comparison of normal-force coefficients obtained from force measurements and from pressure measurements. M = 3.12.

[redacted]